Deciphering the internalization mechanism of WRAP:siRNA nanoparticles

Sébastien Deshayes, Karidia Konate, Marion Dussot, Bérengère Chavey, Anaïs Vaissière, Thi Nhu Ngoc Van, Gudrun Aldrian, Kärt Padari, Margus Pooga, Eric Vivès, et al.

Deciphering the internalization mechanism of WRAP:siRNA nanoparticles.

Sébastien Deshayes[1], Karidia Konate[1], Marion Dussot[1], Bérengère Chavey[1,2], Anaïs Vaissière[1], Thi Nhu Ngoc Van [2], Gudrun Aldrian[2], Kärt Padari[3], Margus Pooga[4], Eric Vivès[1], Prisca Boisguérin[1#]

1 - Centre de Recherche de Biologie cellulaire de Montpellier, CNRS UMR 5237, 1919 Route de Mende, 34293 Montpellier Cedex 5, France

2 - Sys2Diag, UMR 9005-CNRS/ALCEDIAG, 1682 Rue de la Valsière, 34184 Montpellier CEDEX 4, France

3 - Institute of Molecular and Cell Biology, University of Tartu, Riia 23, 51010 Tartu, Estonia.

4 - Institute of Technology, University of Tartu, Nooruse 1, 50411 Tartu, Estonia.

Corresponding author: Prisca Boisguérin, Centre de Recherche de Biologie cellulaire de Montpellier, CNRS UMR 5237, 1919 Route de Mende, 34293 Montpellier Cedex 5, France, tel : 0033 4 34 35 95 26.

Keywords: cell-penetrating peptides, nanoparticle, siRNA delivery, endocytosis, transduction.

ABSTRACT

Gene silencing mediated by double-stranded small interfering RNA (siRNA) has been widely investigated as a potential therapeutic approach for a variety of diseases and, indeed, the first therapeutic siRNA was approved by the FDA in 2018. As an alternative to the traditional delivery systems for nucleic acids, peptide-based nanoparticles (PBNs) have been applied successfully for siRNA delivery. Recently, we have developed amphipathic cell-penetrating peptides (CPPs), called WRAP allowing a rapid and efficient siRNA delivery into several cell lines at low doses (20 to 50 nM).

In this study, using a highly specific gene silencing system, we aimed to elucidate the cellular uptake mechanism of WRAP:siRNA nanoparticles by combining biophysical, biological, confocal and electron microscopy approaches. We demonstrated that WRAP:siRNA complexes remain fully active in the presence of chemical inhibitors of different endosomal pathways suggesting a direct cell membrane translocation mechanism. Leakage studies on lipid vesicles indicated membrane destabilization properties of the nanoparticles and this was supported by the measurement of WRAP:siRNA internalization in dynamin triple-KO cells. However, we also observed some evidences for an endocytosis-dependent cellular internalization. Indeed, nanoparticles co-localized with transferrin, siRNA silencing was inhibited by the scavenger receptor A inhibitor Poly I and nanoparticles encapsulated in vesicles were observed by electron microscopy in U87 cells.

In conclusion, we demonstrate here that the efficiency of WRAP:siRNA nanoparticles is mainly based on the use of multiple internalization mechanisms including direct translocation as well as endocytosis-dependent pathways.

1. Introduction

Small interfering RNAs (siRNAs) represent a wide source of efficient and selective therapeutic molecules that promote the transient reduction of any kind of intracellularly expressed protein, whether they are endogenous or expressed by an infectious agent such as a virus or a bacteria. The first therapeutic siRNA called ONPATTRO™ (Patisiran) has been approved by the FDA in 2018 for the treatment of transthyretin-mediated amyloidosis. In this case, the siRNA is encapsulated within a liposome-based nanoparticle to trigger its delivery to the liver following intravenous infusion [1]. Currently, more than 20 siRNA-based therapies are in clinical trials for a wide variety of diseases (cancer, exogenous infections or genetic disorders). siRNAs, however, remain one of the most sensitive biomolecules suffering from rapid metabolic degradations mediated by RNase all along the "drug delivery route", from the administration site (intestine or blood stream) until the intracellular compartments themselves, where siRNAs need to be ultimately taken in charge by the RISC system to induce a specific degradation of the targeted mRNA [2]. Indeed, the plasma half-life ($t_{1/2}$) for a free siRNA molecule in the blood stream has been calculated to be about only 6 min [3].

Different strategies have been developed to by-pass these bottlenecks of physical stability and efficient delivery. First, different oligonucleotide modifications are available thus reducing or abolishing their sensitivity to nucleases upon anionic charge neutralization, ribose modifications or nucleic acid bond changes [4]. Second, encapsulation of unmodified siRNAs by different polymers also promoted a higher protection from the nuclease degradation. These include poly(lactic-co-glycolic acid) (PLGA), polyethylenimine (PEI) or liposomes (RNAiMAX), three main synthetic molecules used nowadays to deliver siRNAs or DNA molecules whether as native or modified version. Even if being used worldwide as general transfection reagents, the way these compounds enter the cells still remains elusive and sometimes controversial. However, several studies have highlighted that an endocytosis-dependent internalization is privileged for most of these transfection reagents [5–7].

Cell-penetrating peptides (CPPs) have been used as potent transfection agents for more than 30 years and hundreds of studies have been performed in order to identify their mechanism(s) of cellular entry [8,9]. But these investigations have been extremely difficult to bring to an ubiquitous conclusion because of the utilization of a wide panel of different conditions (such as concentration, cell type, formulation, physicochemical properties of the peptide associated to those of the cargo, etc.) [10,11]. However, it is nowadays widely accepted that CPPs internalize mainly *via* endocytosis-dependent pathways (macropinocytosis, clathrin- and caveolin-dependent endocytosis), resulting in a reduced intracellular accessibility of the CPP and its cargo [12–14]. In some cases, depending on the concentration used (e.g. high *versus* low CPP concentration) a direct membrane translocation has also been reported [12,15].

Since several years, we have been interested in the development of amphipathic peptides to complex with and to deliver siRNA into cells [16–19]. Recently, we developed two peptides (WRAP1 and WRAP5) that are capable of self-assembling, in particular with siRNA, into peptide-based nanoparticles (PBNs) of about 80-100 nm diameter [20]. Both peptides with a length of 15 and 16 amino acids, respectively are composed of combinations of three amino acids (W, R, and L). These new peptides both with a net positive charge (+5) showed a rather similar transfection efficacy compared to CADY-K [18] or RICK [19], but they are shorter (3 - 4 amino acids less), made of a reduced set of different amino acids (3 *versus* 7), thus making easier their synthesis. For siRNA transfection, tryptophan residues were shown to be important [21] but we did not see any difference in nanoparticle formation whether they were clustered (WRAP5) or scattered (WRAP1) within the primary sequence.

Both WRAP-PBNs showed a strong capacity to deliver siRNAs into different cell lines, as determined by the specific and efficient silencing of targeted proteins, with up to 90% of inhibition of either overexpressed or endogenous proteins. Since knock-down effects of siRNA-loaded WRAP1 and WRAP5 nanoparticles were nearly identical with those obtained with a RNAiMAX:siRNA formulation, we assumed a similar level of siRNA protection with both reagents during the complete route of transfection, from the extracellular medium till the silencing effect of the siRNA at the RISC system [20]. We have also demonstrated, in a U87 glioblastoma cell line, a rapid cell-association and cell-internalization of Cy3b-siRNA with IC_{50} values peaking at 240 s and 185 s of incubation time for WRAP1 and WRAP5 nanoparticles, respectively. To further understand this apparent fast internalization, we were interested in deciphering the mechanism(s) of cellular entry of our WRAP-based PBNs.

Exploring uptake mechanisms underlying oligonucleotide delivery and intracellular trafficking still remains elusive and cannot be ubiquitously ascertained for all categories of delivery systems and for all used cell types [13]. Therefore, it is important to correlate every internalization pathway with an unambiguous biological read-out triggered by the fraction of the cargo that actually reaches its target. In the case of siRNAs, protein silencing requires the siRNA to be delivered into the cytosol to induce its cellular function (e.g. luciferase knock-down) upon binding to the complementary mRNA sequence.

In this work, we thus investigated with a critical eye all internalization mechanisms susceptible to be followed by our WRAP-PBNs using different strategies that are extensively proposed in the literature to deduce the pathway(s) followed during the intracellular delivery of biomolecules. The first hint of direct translocation was given by a leakage assay using artificial membrane models, such as Large Unilamellar Vesicles (LUV). In parallel, we evaluated the effect of a wide panel of well-defined endocytosis and scavenger receptor A (SR-A) inhibitors on the luciferase expression following WRAP:siRNA-Fluc transfection. We also investigated the potential co-localization of fluorescent PBNs

with widely employed endocytosis markers. In addition, to avoid potential side-effects of endocytosis inhibitors, we also studied delivery of the PBNs in dynamin triple-knock-out murine endothelium fibroblasts (TKO-MEF) [22], thus excluding all active dynamin-dependent internalization processes. Finally, electron microscopy studies was used to establish the subcellular localization of Nanogold™-labelled siRNA complexed with WRAP, specifically whether it is cytoplasmic or endosomal.

Based on the results obtained, we can conclude that WRAP-PBNs are very promising transfection reagents thanks to their ability to enter cells either *via* direct cellular translocation or via an endocytosis-dependent internalization followed by a fast endosomal escape. The combination of these observations explains the fast cytosolic accessibility of the siRNA to specifically silence protein expression at low siRNA concentration.

2. Materials and methods

Details of Materials and Methods are given in the Supplementary Material.

2.1. Nanoparticle formation: Stock solutions of WRAP peptides [WRAP1 (NH_2-LLWRLWRLLWRLWRLL-$CONH_2$) and WRAP5 (NH_2-LLRLLRWWWRLLRLL-$CONH_2$)] were prepared in pure water. siRNA stock solutions were prepared in RNase-free water. Nanoparticle formation was performed in pure water supplemented by 5% (m/v) glucose by adding at room temperature first the peptide and then the corresponding amount of siRNA at molar ratio (R) of 20 (WRAP:siRNA = 20:1). Formulated nanoparticles could be stored for several weeks at 4°C.

2.2. Monolayer techniques (Langmuir): Adsorption consists in the measurement of the peptide-induced surface pressure (ΔΠ) at the air-water interface as a function of peptide concentration in the subphase and is therefore indicative for the air-water interface affinity and amphipathic features of peptides [23]. The maximal concentration for which no further variation of surface pressure is detected corresponds to the critical micellar concentration (CMC). Adsorption at the air-water interface was carried out using an in-house setup, in which surface tension was measured with a Prolabo tensiometer (France) using the platinum plate of the Wilhelmy method [23]. Surface pressure measurements were made at equilibrium after injection of aliquots of an aqueous peptide solution into the aqueous subphase (0.154 M NaCl solution), gently stirred with a magnetic stirrer. To determine the critical micellar concentration (CMC), this procedure was repeated until no further increase in surface pressure could be detected.

2.3. Leakage assay: Large unilamellar vesicles (LUV) composed of DOPC/SM/Chol (4/4/2; mol/mol/mol) were prepared as described in the Supplementary Material section. Fluorescence leakage assay was measured on a PTI spectrofluorometer at room temperature (Ex = 360 nm $\pm$ 3 nm; Em 530 nm $\pm$ 5 nm). In brief, LUVs were diluted in 1 mL buffer (20 mM HEPES, 145 mM NaCl, pH 7.4) to a final concentration of 100 µM. To access the background fluorescence, the LUVs alone were measured during 100 seconds. Thereafter, leakage was measured as an increase in fluorescence intensity upon addition of WRAP1/WRAP5 (2.5 µM) or WRAP1/WRAP5-based nanoparticle (R = 20 using 2.5 µM WRAP) during the next 900 seconds (15 min). Finally, 100% fluorescence was achieved by solubilizing the membranes with 0.1% (v/v) Triton X-100 resulting in the completely unquenched probe (at 1,000 seconds).

2.4. Cell culture conditions: U87, human glioblastoma cells stably transfected with Firefly and Nanoluc luciferase (FLuc-NLuc) encoding plasmid [16] were grown in DMEM-pyruvate-GlutaMAX™ medium (Life Technologies), supplemented with penicillin/streptomycin (Life Technologies), 10 % heat-inactivated fetal bovine serum (FBS, ThermoFisher) and non-essential amino acids (NEAA 1X, LifeTechnologies). Furthermore, hygromycin B (50 µg/mL, Invitrogen) was added as selection antibiotic. TKO-MEF, dynamin-triple KO murine epithelial fibroblasts (kindly provided from the laboratory of Pietro De Camilli, New Haven, CT, United States) were grown in DMEM/F12 medium (Life Technologies), supplemented with L-Glutamine, penicillin/streptomycin (Life Technologies) and 10% heat-inactivated fetal bovine serum (FBS, ThermoFisher). All cells were maintained in a humidified incubator with 5% CO_2 at 37°C.

2.5. Luciferase assay: U87 cells (5,000 cells per well) were seeded, 24 h before experiment into 96-well plates and incubated with the nanoparticles as previously described [20] (see also Supplementary Material). Luciferase activity was quantified using a plate-reading luminometer (POLARstar Omega, BMG Labtech) and half-diluted Dual Luciferase Assay Reagents as described by the manufacturer (Promega). The results were expressed as percentage of relative light units (RLU) for each luciferase, normalized first to non-treated cells (%FLuc and %NLuc) and then to the value of %NLuc to obtain the Relative Luc Activity (%FLuc/%NLuc).

2.5.1. Endocytosis inhibitors / SR-A inhibitors: To evaluate the endocytosis pathways and the potential implication of the SR-A receptors, cells were pre-incubated for 30 min at 4°C or at 37°C with the different endocytosis (30 min) or SR-A inhibitors (60 min) at the indicated concentrations (in 70 µL serum-free or -containing medium). Then, 30 µL nanoparticles (with R=20 using 20 nM siRNA) were added for an incubation period of 1.5 h under the same conditions applied during the pre-incubation step. Finally, the whole medium solution was replaced by 200 µL pre-warmed DMEM supplemented with 10 % FBS (36 h incubation) before performing the luciferase assay as described above.

2.6. Cytotoxicity assay (LDH): The Cytotoxicity Detection Kit^{Plus} (LDH, Roche Diagnostics) was used to evaluate the cytotoxicity induced by the nanoparticles as described previously [20] (see also Supplementary Material).

2.7. Confocal microscopy: 300,000 U87 cells were seeded 24 h before imaging into 35 mm glass bottom dishes (FluoroDish, World Precision Instruments). After the incubation with the WRAP PBN (condition given in the Supplementary Material), live cell images were acquired on an inverted Leica SP5-SMD microscope. Image acquisitions were done sequentially to minimize crosstalk between the fluorophores. Each confocal image was merged and adjusted with the same brightness and contrast parameters using the ImageJ software.

2.7.1. Endocytosis markers: Transferrin-Alexa488 (20 µg/mL final conc.), Cholera Toxin Subunit B-Alexa488 (1 µg/mL final conc.) or pHrodo™ Green Dextran 10.000 MW-green (25 µg/mL final conc.) were added to the medium together with the nanoparticles.

2.7.2. Endosome markers: CellLight™ Early Endosomes-GFP or CellLight™ Late Endosomes-GFP (2.5 µL each) were added to the medium after cell adhesion (at least 16 h before the nanoparticle incubation).

2.7.3. Lysosome marker: LysoTracker™ Green DND-26 (70 nM final conc.) was added to the medium together with the nanoparticles.

2.8. Experiments on TKO-MEF cells:

2.8.1. Spinning disk experiments. TKO-MEF cells were split in two T75 flasks, one with complete medium (= Control condition in Figure 4B) and one with complete medium supplemented with 3 µM 4-Hydroxytamoxifen (OHT, Sigma-Aldrich) (= TKO condition in Figure 4B).

After 48h of incubation in high OHT concentration, cells were maintained in a lower OHT concentration (300 nM) for 3-5 additional days before the experiments for a more complete knockout level. During this time, cells can be split once or twice depending on the confluency and seeded on glass coverslips 24 h prior to imaging. Control cells were handled the same way as KO cells using complete media without OHT addition.

For imaging, cells were seeded onto glass coverslips in 24-well plates (150,000 cell/mL). Before the nanoparticle incubation, the coverslips were washed twice with D-PBS and transferred into a new 24-well plate. Afterwards, cells were incubated with the nanoparticles (WRAP:Cy5-siRNA; R = 20, Cy5-siRNA = 40 nM, in 100 µL DMEM FluoroBrite) for 20 min at 37°C. Control cells were incubated with DMEM FluoroBrite alone. After the incubation, all coverslips were washed twice with D-PBS, transferred in a new 24-well plate and placed on ice (= 4°C). Cells were then incubated with transferrin-Alexa488 (10 µg/mL final conc.) in DMEM FluoroBrite for 15 min at 4°C to allow transferrin to bind with its receptors at the membrane surface. Control cells were incubated in the same way using DMEM

FluoroBrite alone. To allow transferrin internalization, cells were transferred to a 37°C incubator for 5 min. Internalization was stopped and non-internalized transferrin was removed away by immediately performing two washes with cold sodium acetate buffer (50 mM NaAc, 150 mM NaCl pH 4.5). Finally, cells were fixed with 4% paraformaldehyde (PFA, Sigma-Aldrich) at 37°C for 15 min and mounted with poly-(vinyl alcohol) Mowiol^{TM} 4-88 glycerol Tris buffer (Biovalley) on glass slides for imaging.

Images were acquired on a Spinning Disk Nikon eclipse Ti2 Andor Dragonfly 200 using a lens 60x Plan Apo lambda 1.4 NA oil and an EMCCD iXon888 Life Andor camera. Cy5 signal was acquired using the 637 nm laser (30%, exposure time 200 ms) and the 700 nm filter for the emission. Alexa488 signal was acquired using the 488 nm laser (6%, exposure time 200 ms) and the 520 nm filter for the emission. Multi-position acquiring was performed in a z-scan mode (22 z-scans with a step size of 0.2 µm). All images were adjusted with the same brightness and contrast parameters with the ImageJ software.

2.8.2. Fluorescence spectrometry experiments. TKO-MEF cells were split and seeded directly into 24-well plates as described above. Nanoparticle and transferrin incubation as well as all washing steps were performed with one control and one TKO condition as described above. After the cold sodium acetate buffer washing steps, cells were trypsinized (100 µL 0.05% trypsin-EDTA, Life Technologies) to remove membrane-bound nanoparticles (10 min at 37°C). To stop trypsinization, 400 µL D-PBS containing 5% FBS were added. Cell suspensions were transferred in Eppendorf tubes and centrifuged (13.500 rpm, 10 min, 4°C). Supernatants were removed and replaced by 100 µL RIPA lysis buffer (50 mM Tris, 150 mM NaCl, 1.0% Triton X-100, 0.1% SDS, pH 8.0) containing protease inhibitors (SigmaFAST, Sigma-Aldrich). Cell lysis was performed during 30 min under agitation at 4°C. After a centrifugation step (13.500 rpm, 10 min, 4°C), 50 µL supernatant were transferred to a black ½ area 96-well plate (Greiner) for fluorescence acquisition using a plate reader (POLARstar Omega, BMG): Cy5 (Ex 650 nm/Em 666 nm) and Alexa488 (Ex 490 nm/Em 525 nm). Fluorescence intensities were normalized upon protein concentration which was quantified using the Pierce BCA Protein Assay (ThermoFisher).

2.9. Transmission electron microscopy: siRNA was tagged with nanogold (NG) cluster (Monomaleimido Nanogold, Nanoprobes, NY, d 1.4 nm) *via* a thiol group followed by conjugate purification as described earlier [24]. NG-labeled siRNA was complexed with WRAP1 or WRAP5 (R = 20, 80 nM siRNA) and U87 cells were incubated with the resulting nanoparticles for 10-15 min or 1-2 h. The specimens were fixed with glutaraldehyde and the NG-label on siRNA was revealed by magnification by silver as described earlier [25]. The specimens were embedded in epoxy resin (TAAB Laboratories Equipment Ltd., UK), cut into ultrathin sections, and contrasted with uranyl acetate and lead citrate. The sections were examined with FEI Tecnai G2 Spirit transmission electron microscope (FEI, Eindhoven, Netherlands) at 120 kV acceleration voltage.

3. Results

3.1. Membrane interaction of WRAP peptides as first contact for cellular internalization.

One of the crucial events occurring during the cellular internalization of peptide-based nanoparticles (PBNs) is certainly their direct contact with the cellular membrane. The combination of charges and amphipathicity of WRAP peptides is considered to be the basis of the cell-penetrating effect [20]. We thus investigated the ability of both WRAP peptides to interact with an air-water interface and with large unilamellar vesicles (LUVs). We previously showed by structure prediction studies that hydrophilic and hydrophobic area repartition revealed a pronounced amphipathic character for both peptides [20]. With Langmuir techniques, this amphipathicity was quantified by an adsorption test where the affinity for the air-water interface that imitated the interfacial environment of a membrane was assessed (**Figure 1A**). Adsorption of WRAP1 was characterized by a critical micellar concentration (CMC) of 190 nM and a high saturating surface pressure (Πsat) of 33 mN/m, whereas, the adsorption of WRAP5 peptide had a surprisingly low CMC of 92 nM with a Πsat of 31 mN/m, similar to WRAP1. Compared to the previously reported RICK peptide (CMC ~100 nM, Πsat ~35 mN/m [19]) WRAP5 seems to have a more pronounced amphipathic character than WRAP1 (based on different CMC with similar Πsat).

LUVs with a lipid composition [DOPC/SM/Chol (2:2:1)] reflecting the plasma membrane [26] were used to directly evaluate the possibility of lipid bilayer interaction and/or transduction properties of nanoparticles. To follow the WRAP-induced leakage of the lipid membrane, LUVs were generated in order to encapsulate both a fluorescent dye and a quencher (Scheme in **Figure 1B**). In the absence of peptides (or nanoparticles), no leakage was observed (baseline during the first 100 s). Addition of both free peptides on the LUVs induced a significant increase in fluorescence revealing an important leakage in a dose-dependent manner (**Figure S1**). After 15 min, a leakage of 46±5% and of 62±12% compared to the Triton condition (positive control) was obtained at the highest used concentration (2.5 µM) for WRAP1 and WRAP5 peptides, respectively. This is in agreement with a partially higher grand average of hydropathicity (GRAVY) calculation (ProtParam, Expasy website) showing a more pronounced hydrophobic character of WRAP5 (0.647) compared to WRAP1 (0.550). In contrast, when both peptides were assembled with the siRNA as nanoparticles, the leakage was 1.3-fold weaker (36±2%) for WRAP1:siRNA and 1.5-fold weaker (42±12%) for WRAP5:siRNA compared to the free corresponding peptides (**Figure 1C, D**). Similar leakage values have been reported for the RICK peptide (60%) or the RICK:siRNA PBN (28%) [19]. In both cases, this could be explained by the fact that, in complexes, a

substantial part of the peptide is involved in direct interactions with the siRNA, reducing the peptide availability for interactions with lipids.

In conclusion, this work and our previously published data [20] suggest that the WRAP peptide forms small nanoparticles (~30 nm) in the presence of siRNA which are able to further self-assemble to larger ones of ~80 nm. Due to the higher molar ratio (R = 20) of WRAP peptides compared to siRNA, we conclude that the siRNA is fully encapsulated in stable nanoparticles showing a positive global surface charge (Zeta potential of 30-40 mV) and highly protected from degradation as previously shown for the RICK peptide [19]. Finally, the amphipathic character of WRAP peptides allows first the formation of the nanoparticle in the presence of siRNA and secondly the interaction with the cell membrane and the subsequent internalization of the siRNA.

3.2. Inhibition of endocytosis did not alter WRAP:siRNA nanoparticle activity.

In our previous publication [20], we have shown that both WRAP:siRNA PBNs were internalized in cells within 15 min, which could suggest a direct cell membrane translocation, as deduced from the leakage results. To verify whether the main endosomal pathways were involved or not in the WRAP:siRNA PBNs internalization, we evaluated the biological efficiency of WRAP:siRNAs PBNs delivery in different conditions (**Figure 2A**).

First, we revealed a specific silencing efficacy of around 80% under standard conditions (37°C) for both nanoparticles while the scrambled siRNA (siSCR) version induced no~~ne~~ effect (**Figure 2B**). Afterwards, we downregulated the energy-dependent pathways by incubating the cells either at 4°C or under ATP depletion (NaN_3/2-Deoxy-Glucose at 37°C) to compare the luciferase knock-down efficiency to that of the standard 37°C incubation. To ensure ~~the~~ full energy depletion, cells were pre-incubated for 30 min under the respective conditions before the addition of the siRNA-FLuc loaded nanoparticles for an additional 90 min incubation. After medium replacement to avoid toxicity of the endocytosis inhibitors (NaN_3/2-Deoxy-Glucose), cells were further incubated for 36 h at 37°C. No specific washing steps or addition of enzymes (RNase or protease) were used due to measurement of luciferase expression in different inhibitory conditions relative to the normal condition. Determination of luciferase protein silencing (~80% of knock-down) revealed that both PBNs efficiently induced luciferase knock-down in an energy-independent environment such as at 4°C or under ATP depletion in a comparable manner to the standard conditions (ns between groups *versus* siFLuc at 37°C) (**Figure 2B**).

To confirm the implication of an energy-independent cellular mechanism, internalization of both WRAP:siRNA complexes was evaluated in the presence of specific chemical inhibitors of different endocytosis pathways. As described above, endocytosis inhibitors were pre-incubated for 30 min prior

to the addition of the nanoparticles as recommended to ensure an effective inhibition of the endocytotic pathway [10]. The luciferase silencing was then quantified compared to the standard conditions after the substitution of the inhibitor solutions by medium completed with 10% serum.

Different well-known endocytosis inhibitors were used. These include chlorpromazine (CPZ - clathrin-dependent endocytosis inhibitor), nystatin (NYS - disrupting caveolar structures and functions), 5-(N-ethyl-N-isopropyl)amiloride (EIPA - macropinocytosis inhibitor), wortmanin (WORT - macropinocytosis inhibitor) and methyl-β–cyclodextrin (MBCD – lipid raft inhibitor) (for a review see [27]). For each inhibition condition, we verified the potential toxicity of the different inhibitors in our cellular system and we selected for each one the highest concentration without any significant toxic effect (data not shown). As summarized in **Figure 2C**, both nanoparticles were still effective in the presence of the different endocytosis inhibitors and showed a similar knock-down compared to the standard condition (ns between groups *versus* no inhibitor). Moreover, luciferase activity remains the same when scrambled siRNA (siSCR) was delivered using the same systems.

If WRAP PBN luciferase silencing effect was still observable at the same level under energy depletion (4°C or NaN_3/2-Deoxy-Glucose), a statistically non-significant increase in luciferase activity (~15%) was observed for WRAP5:siRNA when using endocytosis inhibitors NYS, CPZ and MBCD. Intriguingly WRAP1:siRNA nanoparticles showed the same knock-down activity with or without inhibitors. However, at this point, we cannot exclude that endocytosis-dependent internalization could be partially implicated in WRAP5 internalization. Furthermore, it is also possible that luciferase silencing could be due to a limited amount of nanoparticles sticking at the cell membrane which internalized after endocytosis inhibitors were removed.

3.3. WRAP:siRNA nanoparticles did not co-localize with markers of caveolin-mediated endocytosis or of macropinocytosis.

Investigations of mechanisms of cellular internalization of non-viral delivery systems were performed using different chemical inhibitors of endocytosis [5,13,14,28]. A number of these were described to be specific for the targeted pathways but increasing evidences suggest that they lack specificity and may give misleading results [29,30]. Because, it is also possible that WRAP PBN silencing activity is due to nanoparticles sticking at the cell membrane which internalized after endocytosis inhibitors were removed, we further evaluated the internalization of both PBNs by confocal microscopy using three specific endocytosis markers [31]. As representative endocytosis markers, we selected transferrin, cholera toxin subunit B (CtB) and dextran for localizing the clathrin-dependent, the caveolin-mediated pathway and the macropinocytotic pathways respectively (see schema **Figure 3A**).

The co-localization experiments were performed using WRAP5-based nanoparticles loaded with fluorescent labelled siRNA (siRNA-Cy5) co-incubated for 60 min with the corresponding endocytosis markers. For the CtB and dextran conditions, we observed nearly no significant co-localization with siRNA-Cy5, confirming that these pathways are not exclusively used for the internalization (**Figure 3B**). For the transferrin condition, results were less clear. First of all, when Alex488-transferrin was taken up in the absence of WRAP5:siRNA PBNs (**Figure 3A**) the cytosolic distribution corresponded to the patterns previously shown on U87 cells by Dixit et al. [32]. In the presence of WRAP5:siRNA PBNs, after 60 min of incubation we observed a clear co-localization of both molecules suggesting an internalization *via* clathrin-dependent endocytosis (**Figure 3C**). Variation of the incubation time to shorter periods (30 min and 10 min) revealed a time-dependent increase over the incubation time of co-localization of fluorescence-labelled siRNA and Alexa488-transferrin in U87 cells. These results are in contradiction with the fact that chlorpromazine as an inhibitor of the clathrin-dependent endocytosis induced no significant effect on luciferase silencing for the WRAP5:siRNA nanoparticle. We therefore cannot exclude that the detection level between the fluorescence microscopy experiment and the biological evaluation of the knock-down activity could reflect an important difference in the quantity of the siRNA detected in the endosomal structures or actually delivered into the cytoplasm. In addition, we are aware of a potent bias in the result interpretation due to siRNA degradation or siRNA-label cleavage.

Finally, experiments performed with the WRAP1:siRNA-Cy5 PBNs showed the same co-localization pattern as observed for WRAP5:siRNA-Cy5 PBNs (**Figure S2**).

3.4. WRAP:siRNA nanoparticles internalized in dynamin triple KO cells.

To better understand the previous results regarding the transferrin co-localization, we performed additional experiments related to clathrin-mediated endocytosis, a very well-characterized process whose functions in eukaryotes involved the internalization of cell surface molecules and extracellular materials [33]. Clathrin-mediated endocytosis is a highly coordinated process that begins with the assembly of clathrin-coat components at the plasma membrane through interactions with plasma membrane lipids and proteins destined for recycling by this endocytic pathway. The nascent bud grows and invaginates with the assistance of multiple accessory factors and the budding vesicle is finally released into the cytoplasm *via* a dynamin-mediated, membrane-fission reaction [34]. Mammalian genomes contain three dynamin genes (*DNM1, DNM2 and DNM3*). The three proteins, dynamin 1, 2 and 3, share 80% overall homology and play in part redundant roles during the membrane fission reaction of clathrin-mediated endocytosis [35].

We thus used dynamin Triple Knock-Out (TKO) mouse embryonic fibroblasts obtained from conditional KO cells upon tamoxifen-induced gene recombination [22]. These cells were incubated with WRAP:siRNA-Cy5 PBNs alone, with transferrin-Alexa488 alone or with both entities to evaluate their relative internalization, either in native (control = non-treated) or dynamin TKO condition (treated with 4-Hydroxytamoxifen).

Spinning disc confocal microscopy was performed to visualize the location of transferrin-Alexa488 and of the siRNA-Cy5 loaded PBNs in control and dynamin TKO cells. Representative images shown in **Figure 4A** showed a clear punctuated transferrin pattern in the control condition reflecting its clustering in clathrin coated pits/vesicles. In contrast, a weak and diffuse background fluorescent signal of transferrin-Alexa488 due to the lack of transferrin recruitment at clathrin coated pits was observed in the TKO condition. These results were identical with those presented by Ferguson *et al.* for the dynamin double KO cells [36] or by Park *et al.* for the TKO cells [37] validating the applied experimental conditions. Interestingly, both cell types exhibited a similar fluorescent pattern of the internalized siRNA-Cy5, showing that WRAP PBN uptake was independent from clathrin-mediated and dynamin-dependent endocytosis.

Overall fluorescence quantification of cell lysate from all conditions shows that both nanoparticles were able to translocate the siRNA-Cy5 through the membrane of living cells having no dynamin-dependent endocytic processes to the same extent as the control cells (TKO *versus* control conditions) (**Figure 4B**). Curiously, we could not observe any differences in the transferrin-Alexa488 translocation between both cell types. We assumed that the amount of internalized transferrin-Alexa488 (control condition) corresponded to those sticking at the cell membrane (TKO condition), resulting in the same Alexa488-signal intensity after cell lysis.

Finally, as an additional control experiment, we used the small molecule dynamin inhibitor, hydroxy-dynasore (HD), to produce a robust impairment of fluid phase endocytosis and peripheral membrane ruffles [22]. To ensure full dynamin inhibition, U87 cells were pre-incubated for 60 min with HD before the addition of the WRAP1:siRNA or WRAP5:siRNA-FLuc nanoparticles. Quantification of the luciferase protein silencing (~80% of knock down) revealed that both PBNs efficiently induced luciferase knock-down in a dynamin-independent manner (ns between HD *versus* siFLuc) (**Figure S4**), confirming results obtained on TKO cells.

3.5. WRAP:siRNA nanoparticle internalization is probably not mediated by SR-A receptors

The investigation of uptake mechanisms for cell-penetrating peptides or PBNs is an ongoing project which spans a time period over more than two decades. So far, it is not possible to give a universal answer because the uptake mechanism seems to be dependent on a multitude of factors such as the peptide used, the nature of the cargo, the cell type, etc [10]. Some years ago, the group of Prof. Langel demonstrated that the scavenger receptor A (SR-A), a transmembrane receptor, was involved in the uptake of nanoparticles formed by PepFect, another CPP family member [38–40].

To evaluate the potential involvement of the SR-A receptor in the uptake of WRAP nanoparticles several poly-anions such as polyinosinic acid (Poly I), fucoidan (Fuco) or dextran sulfate (DexS) can be used as inhibitors, while polycytidylic acid (Poly C), galactose (Gala) and chondroitin sulfate (ChonS) can be used as well as their respective controls because of their similar structure and their lack in SR-A affinity [40]. First we confirmed, using an agarose gel shift assay, that the poly-anions (Poly I, Fuco and DexS) did not destabilize WRAP:siRNA nanoparticles (**Figure S5**). Afterward, WRAP:siRNA efficiency was evaluated on U87 cells in the presence of the three SR-A inhibitors as well as their respective controls. A pre-incubation of the cells for 60 min at optimal concentration of the inhibitors [41] were performed before the addition of WRAP:siRNA PBNs for further 90 min. After the medium replacement to avoid cell toxicity, cells were incubated for 36 h in complete medium.

Quantification of the luciferase protein silencing under the serum-free incubation confirmed that co-treatment of cells with SR-A poly-anion controls (Poly C, Gala or ChonS) did not influence the gene silencing abilities of the WRAP-based siRNA-Fluc PBNs (ns *versus* no inhibitor) (**Figure 5A**). In the same way, the SR-A inhibitors Fuco and DexS have no effect on luciferase knock-down activity. In contrast, Poly I increases luciferase activity from ~8% to 60% for WRAP1:siRNA and to 39% for WRAP5:siRNA(**Figure 5A**) during the serum-free incubation.

Because the interaction between the nanoparticles and the SR-As could be modified by the presence of serum proteins in the incubation medium, the same experiment was performed with

complete medium (**Figure 5B**). First, we observed a slight increase of the expression of the luciferase from ~8% without serum to 18±5% for WRAP1:siRNA and to 28±1% for WRAP5:siRNA resulting from the presence of serum. This observation could be due to the dynamic adsorption of serum proteins at the cellular surface and/or to the WRAP:siFLuc nanoparticles thus providing a "protein corona" interfering with the PBN/cell membrane interactions. As shown previously in **Figure 5A** for the serum-free condition, Poly C, Gala and ChonS as well as Fuco and DexS have no effect on the luciferase silencing property of WRAP:siRNA. In contrast, for the Poly I condition we observed nearly the same luciferase activity for WRAP1:siRNA independent of the absence or the presence of serum (60±10% *versus* 74±9%, p=ns) and a significant increase in luciferase activity for WRAP5:siRNA (39±7% *versus* 71±5%). In the presence of serum, the SR-A Poly I inhibitor seems to have a higher impact on WRAP5:siRNA internalization compared to WRAP1:siRNA. In parallel, evaluation of all incubation conditions (LDH assay) revealed no effect on cell viability.

In conclusion, even if two of three specific SR-A inhibitors Fuco and DexS do not induce an increase in the level of the reporter gene activity, it is possible that WRAP nanoparticles internalized via SR-As since a lower siRNA activity in the presence of the Poly I with or without serum is recorded. This effect was more pronounced for WRAP5 than for WRAP1 nanoparticles.

3.6. WRAP:siRNA nanoparticles were not found in endosomes or in lysosomes.

Endocytosis generates small (60–120 nm) membrane vesicles that drive various cargo molecules from the plasma membrane of eukaryotic cells into the cytoplasm [34]. Components that have been endocytosed by several pathways are delivered to a common early endosome (EE). The EE compartment is a major cellular sorting station from which cargo molecules can either be trafficked to the late endosomes (LE) and then to the lysosome for degradation, or be returned to the plasma membrane by various routes [42,43]. Using specific EE, LE and lysosome markers we investigated whether WRAP:siRNA nanoparticles were internalized via an endocytosis-dependent pathway or not.

For that purpose, cells were first incubated with fluorescent EE and LE markers at least 16 h before the nanoparticle transfection as recommended by the manufacturer (**Figure 6A**). Afterwards, WRAP5:siRNA-Cy5 PBNs transfection was performed. For both endosomal markers, we could not distinguish any co-localization with the fluorescent siRNA (**Figure 6B**). Especially, the different cellular localization of the siRNA-Cy5 and the EE marker confirmed the previous results and underlined a direct translocation. However, we could not exclude that WRAP5 PBNs bypass the formation of these organelles (e.g. macropinocytosis) or that an early endosomal release of the siRNA in the cytosol occurs. Finally, we also evaluated a specific fluorescent-labelled lysosome marker alone (**Figure 6A**) as

well as its potent co-localization with the WRAP5-vectorized fluorescent siRNA (**Figure 6B**). As expected from results obtained from endosomal labelling, co-incubation of WRAP5 PBN for 60 min did not reveal any co-localized pattern of the lysosome fluorescence dye.

Identical results were obtained using the WRAP1:siRNA-Cy5 PBN co-localization experiments performed with EE, LE and lysosomal markers (**Figure S3**).

3.7. WRAP:siRNA nanoparticle internalization occurs via multiple routes.

To better understand the mechanism behind the WRAP:siRNA PBN internalization, transfected cells were analyzed by transmission electron microscopy (TEM). First of all, control experiments using negative staining confirmed that the addition of the nanogold (NG)-label did not affect the nanoparticle formation or their morphology (data not shown). Afterwards, U87 cells were transfected with WRAP:siRNA-nanogold (NG) during a period of 10-15 minutes or 1-2 hours before cell fixation. WRAP:siRNA-NG nanoparticles avidly associated with the cells, interacted with the cell membrane and were found inside the cell (**Figure 7**). In closer detail, particles interacting directly with the cell membrane were identified (triangles in **Figure 7B, D, F** and **H**), as well as internalized particles in the cytoplasm with no surrounding membrane (stars in **Figure 7B, D, F** and **H**). However, major part of the nanoparticles were found inside vesicles of different sizes (arrows in **Figure 7D and H**), indicating that endocytosis-dependent uptake mechanisms were also implicated. Based on the observed invagination pattern of the U87 cells, we assumed that macropinocytosis could be also implicated in WRAP:siRNA internalization, even if we could not observe any inhibiting effect of both macropinocytosis inhibitors (EIPA and Wortmanin) during luciferase assay (**Figure 2C**).

Moreover, it is also possible that WRAP PBNs could induce plasma membrane activity reorganization by triggering both formation of invaginations and protrusions. However, data from leakage assay indicated that both WRAP:siRNA are able to destabilize LUV reflecting the membrane composition of endosomes in terms of lipid composition (**Figure S6**) meaning that the nanoparticles were potentially able to escape from endosomal encapsulation in a rapid manner.

4. Discussion

The WRAP family of cell-penetrating peptides was designed to increase the efficiency of cell-internalization and to overcome endosomal sequestration of CPP:siRNA by favoring direct translocation [20]. WRAP1 and WRAP5 are very effective for transfection *in vitro* but little is known about their internalization mechanism. We previously reported a maximal intracellular fluorescence

(95% ± 5%) after ~15 min of incubation and IC50 values of cell-internalized Cy3b-siRNA (50%) after 240 and 185 s incubation for WRAP1 and WRAP5 nanoparticles, respectively. This rapid cellular internalization could indeed suggest that i) our WRAP-based nanoparticles are internalized via a direct translocation through the plasma membrane, and ii) our PBNs could rapidly escape from endosomes after endocytosis-dependent internalization.

Experiments at an air/water surface demonstrated that the affinity for a hydrophilic/hydrophobic interface was nearly identical for both peptides (same Πsat) but that the amphipathicity was higher for WRAP5 than for WRAP1 as revealed by a higher CMC (**Figure 1A**). Because both peptides are structured in an α-helical conformation in the presence of siRNA [20], the amino acid composition is mainly responsible for CMC determination. Both peptides have eight leucine and four arginine residues, meaning that the amount of tryptophan residues (four *versus* three for WRAP1 and WRAP5, respectively) as well as their placement within the sequence determine the CMC. Only few publications showing CMC or Πsat values are available such as some work with TP10, PepFect3 and PepFect6 [44]. However, even if the measured PepFect6 Πsat value (32.7±0.5 mN/m) corresponds to those obtained for the WRAP peptides, the CMC value is, at around 500 nM extremely high, underlining the amphipathic character of our peptide. The same is observed for the C6 and C6M1 peptides but with differences in CMC values due to different mathematical approaches [45]. Thus, this strong amphipathic character demonstrated high potential of both WRAP peptides to interact with the interfacial environment of the membrane bilayer.

Since peptide/lipid interactions are essential for cell internalization, we have evaluated and compared the lipid membrane destabilization property of both peptides, alone or as nanoparticle. As shown for other CPPs also forming nanoparticles in the presence of oligonucleotides [19,44,46], we demonstrated that both WRAP peptides induced very potent membrane leakage in LUVs. Identically, the leakage was ~1.4-fold lower once the peptides were complexed with the siRNA (**Figure 1B**).

Because, we did not observe any specific cell toxicity or changes in cell morphology [20], we estimate that the observed leakage of LUVs is a result of pore-like structure formation rather than LUV disintegration. This is in agreement with previous giant unilamellar vesicle (GUV) incubation with RICK-Cy3b-siRNA at nearly identical concentration showing no vesicle destruction on confocal images [19].

Whether the CPP or peptide-based nanoparticle (PBN) internalization occurs via direct translocation or by endocytosis, the initial contact between most CPPs and the cell involves proteoglycans. Nowadays, it is well established that cell-surface heparan sulfate proteoglycans (HSPGs) capture the extracellular CPPs based on electrostatic interactions, ultimately leading to peptide concentration at the cell surface following by peptide uptake at multiple sites of the cell surface [47].

Afterwards, they are internalized via endocytosis or direct translocation probably depending on the nature of the delivery system, on their affinity to lipids and on the cell type [48]. This variability stresses the necessity of studying the internalization mechanism of non-viral gene carriers and to quantify the contribution of each endocytic pathway compared to the overall cellular uptake, in order to elucidate the corresponding intracellular pharmacokinetic model [14].

Applying different endocytic inhibitors to the U87 glioblastoma cells, we first showed that endocytosis-dependent pathways were not the major uptake pathway for WRAP:siRNA nanoparticles (no significant effect on luciferase silencing compared to untreated cells, see **Figure 2C**). In the same manner, changing the cell energy state by lowering the temperature or adding sodium azide exhibited no effect on luciferase silencing, indicating that a direct translocation route was most likely (**Figure 2B**) and privileged in these conditions. Because we are aware that nanoparticles sticking at the cell membrane could further internalize during the following 36 h incubation, under the standard conditions needed for monitoring luciferase silencing, we performed additional confocal microscopy experiments in the presence of "classical" fluorescence-labelled endocytosis markers such as transferrin, cholera toxin subunit B and dextran (**Figure 3** and **Figure S2**) as well as in the presence of early/late endosome or lysosome markers (**Figure 6** and **Figure S3**). With one exception, no co-localization of the WRAP PBNs could be observed in U87 cells with the different markers assuming a direct translocation of our nanoparticles. However, the only co-localization was observed with Alexa488-transferrin indicating a potent clathrin-dependent endocytosis, which is in contradiction with our result observed in the presence of chlorpromazin. To obtain more information on this fact, we performed experiments on chemically inducible dynamin triple-knockout (TKO) MEF cells showing no more transferrin internalization [22]. It is well known that the GTP hydrolysis–dependent conformational change of dynamin assists in membrane fission, leading to the generation of endocytic vesicles [37]. Using these cells, we demonstrated that the WRAP:siRNA-Cy5 nanoparticles were able to translocate the cell membrane even if the main clathrin-mediated or dynamin-dependent endocytic events are not active. However, by blocking one endocytosis pathway, it is always possible that other pathways are upregulated as shown by an increased dextran uptake (marker of-macropinocytosis) in TKO cells compared to control cells [22].

Class A scavenger receptor (SR-A)-dependent internalization was postulated as general mechanism for the cellular uptake of some CPP-based nanoparticles. This was especially observed for PepFect and NickFect based nanoparticles having both a negative zeta potential in the transfection medium, making direct membrane contacts or HSPGs interaction as initial contact unlikely due to charge repulsion [24,38,49,50]. The same effect was also observed for some peptide-morpholinos (PPMO) such as the B-peptide coupled to PMO [41]. In contrast to that, we showed that the silencing

property of WRAP:siRNA nanoparticles was not perturbed using SR-A inhibitors such as fucoidan or dextran sulfate in the absence or in the presence of serum proteins (**Figure 5**). Only the Poly I SR-A inhibitor has a negative impact on WRAP:siRNA nanoparticle silencing which could be explained by a potent SR-A dependent U87cell internalization of the nanoparticles. However, it is difficult to conclude if SR-As are really implicated in their internalization based on the observed Poly I effect because this pharmacological inhibitor also has other targets (class C, E and F scavenger receptors) [41].

Transmission electron microscopy (TEM) is an informative and valuable tool for examining the mechanisms of internalization of PBNs. Using Nanogold™ tag molecules (e.g. siRNA), TEM techniques enable the visualization of siRNA-loaded nanoparticles and to follow their association with cells as well as their intracellular localization. For the WRAP:siRNA-NG complexes, we could observe a rapid interaction with the cell membrane (within 10-15 min) followed by the nanoparticle internalization confirming the rapid cellular transfection previously observed by confocal microscopy (spinning disk technique) [20]. Within the cell, we observed the siRNA-NG mainly in vesicles and to some extent also in the cytosol. Based on these results, we could deduce that our WRAP:siRNA nanoparticles are also internalized by endocytosis-dependent pathways followed be a rapid endosomal escape and cytosol release.

Recently, Walrant and co-workers proposed a model of internalization mechanisms of different CPPs based on the nona-arginine peptide and its analogues with increasing number of tryptophan residues [51]. They divided the peptides into three classes: 1 - peptides with no or one tryptophan making a phase-transfer-like translocation, 2 - peptides with 3 tryptophan residues employing the direct translocation through leaky defects and 3 - peptides with 4 tryptophan residues using membrane-disruptive direct translocation. We partially agree with this model based on our results. We previously reported that siRNA transfection is increased with higher number of tryptophan residues in the peptide sequence (WRAP4 (2 W) < WRAP5 (3 W) ≤ WRAP6 (4 W) [20]. Counter-intuitively, the position of the tryptophan residues (grouped in the primary sequence or clustered through secondary structure adoption) seems not to impact PBN formation and internalization [20] as well as the cellular internalization mechanism as reported herein. WRAP1 (4 W) and WRAP5 (3 W) PBNs internalized in cells with the same rapidity and efficiency without any cytotoxic effect through a mixture of direct membrane translocation and endocytosis-dependent pathways.

As summarized in **Figure 8**, the presented results demonstrate that WRAP:siRNA nanoparticles employ different internalization mechanisms including direct translocation as well as endocytosis. Indeed, several publications revealed that CPPs could internalize *via* both routes depending on the applied CPP concentration, the CPP charge or the size of the cargo [15,52]. More recently, it was

evidenced that tryptophan-rich CPPs (also harboring three W) could be internalized *via* both routes, direct translocation and endocytosis [51]. This is confirmed in our presented study. Nevertheless, it is often difficult to determine “the” predominant used internalization pathway because: i) different uptake routes could be used in parallel and ii) inhibitors could favor one internalization mechanism over the others [13].

Endocytotic processes occur over the whole cell membrane in a continuous manner (e.g. one new clathrin-coated pit per square micron every 2 min [53]) with moderate (20-130 s) or fast kinetics (1-10s) resulting in half of the cell membrane recycled within a few minutes [54]. Therefore, it is evident that nanoparticles could be also internalized via endocytosis after their first cell membrane contact. However, because WRAP PBNs are still active at 4°C or under ATP-depletion, we could not exclude a direct cell translocation of the nanoparticles.

In conclusion, the advantage of the WRAP:siRNA nanoparticles lays in their capacity to direct translocate cell membranes and/or to rapidly escape from endosomes after an endocytosis-based internalization (**Figure S6**). In both cases, this explains the great observed silencing activity of the nanoparticles at low siRNA concentration as reported previously [20].

Acknowledgements

We acknowledge the imaging facility MRI, member of the national infrastructure France-Bioimaging supported by the French National Research Agency (ANR-10-INBS-04, “Investments for the future”), and especially Sylvain De Rossi and Orestis Faklaris for technical advices. This work was supported by the Fondation pour la Recherche Médicale (DBS 79620140930769), the fondation “La Ligue contre le Cancer”, the “Fondation ARC pour la Recherche sur le Cancer” and the "Centre National de la Recherche Scientifique" (CNRS). Electron microscopy experiments and K.P. and M.P. were supported by the Estonian Research Council (PUT1617).

Figure legends:

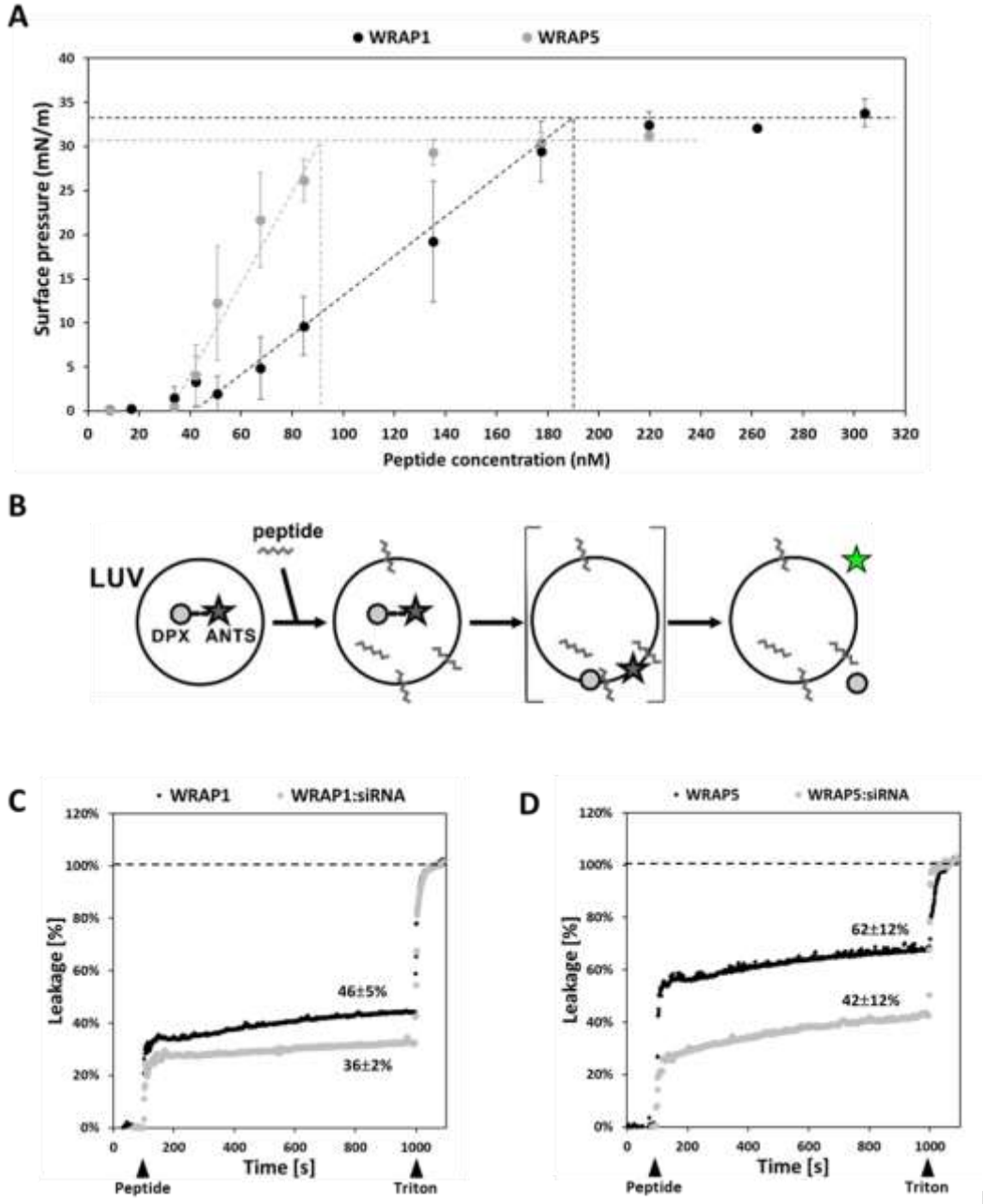

Figure 1. Membrane interaction of WRAP peptides.

A. Adsorptions of WRAP1 and WRAP5 peptides at the air-water interface were graphically represented as the variation of the peptide-induced surface pressure (ΔΠ) as a function of the peptide concentration into the aqueous subphase (mean±SD of 3 independent experiments). Dotted lines indicate the critical micellar concentration (CMC, in nM) and a high saturating surface pressure (in mN/m).

B. Schema representing the principle of the leakage assay.

C and D. Comparison of the leakage properties of WRAP alone (2.5 µM) and WRAP:siRNA (2.5 µM:125 nM) PBNs on LUVs [DOPC/SM/Chol (2:2:1)]. Peptides/nanoparticles were injected at 100 s and the Triton (positive control) at 1000 s (n ≥ 4).

A

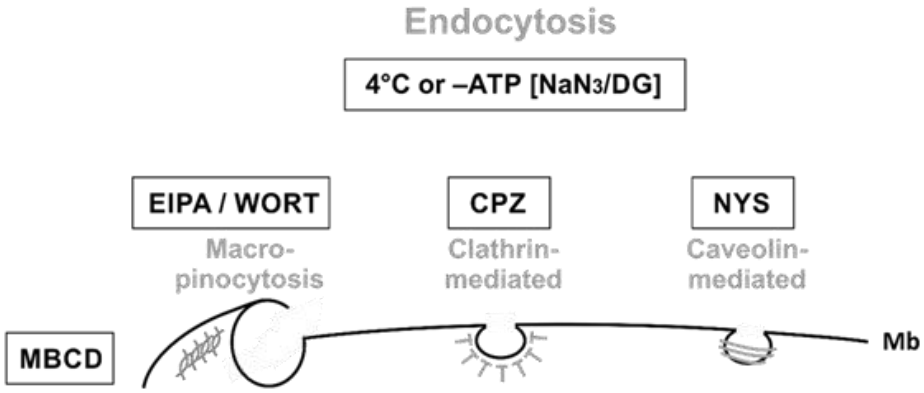
Endocytosis
4°C or –ATP [NaN3/DG]
EIPA / WORT
Macro-pinocytosis
CPZ
Clathrin-mediated
NYS
Caveolin-mediated
MBCD
Mb

B

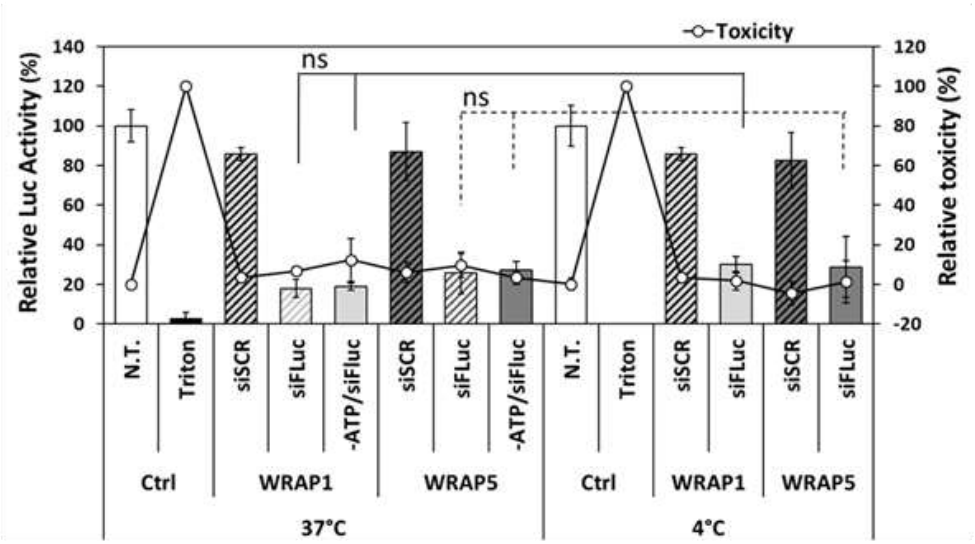
Toxicity
Relative Luc Activity (%)
Relative toxicity (%)
ns
ns
N.T.
Triton
siSCR
siFLuc
-ATP/siFluc
Ctrl
WRAP1
WRAP5
37°C
4°C

C

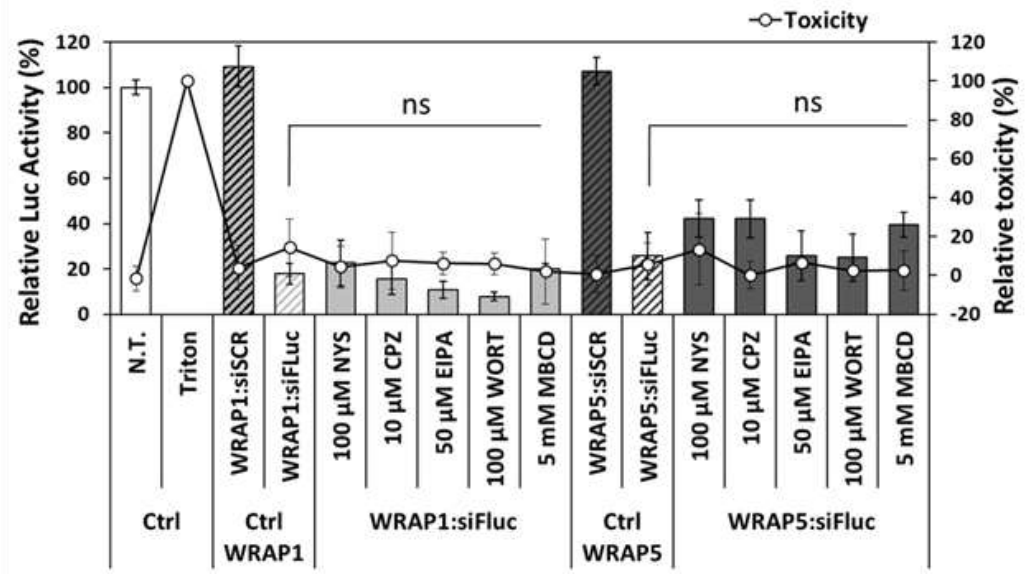
Toxicity
Relative Luc Activity (%)
Relative toxicity (%)
ns
ns
N.T.
Triton
WRAP1:siSCR
WRAP1:siFLuc
100 µM NYS
10 µM CPZ
50 µM EIPA
100 µM WORT
5 mM MBCD
WRAP5:siSCR
WRAP5:siFLuc
Ctrl
Ctrl WRAP1
WRAP1:siFluc
Ctrl WRAP5
WRAP5:siFluc

1

Figure 2: Evaluation of the internalization mechanism of WRAP:siRNA nanoparticles using a luciferase silencing screen.

A. Schema of the different endocytosis pathways and the corresponding inhibitors: 4°C incubation or NaN_3/2-Deoxy-Glucose (DG) for ATP depletion (-ATP), nystatin (NYS) for caveolin-dependent endocytosis, chlorpromazine (CPZ) for clathrin-dependent endocytosis, 5-(N-ethyl-N-isopropyl)-amiloride (EIPA) and wortmanin (WORT) for macropinocytosis as well as methyl-β-cyclodextrin (MBCD) for lipid-raft induced internalization.

Quantification of Luciferase silencing in U87 cells after incubation at 4°C or under ATP-depletion (NaN_3/2-Deoxy-Glucose) (**B**) or with the corresponding endocytosis inhibitors (**C**) in the presence of WRAP:siRNA PBNs (with R=20 using 20 nM siRNA). Under the presented conditions, WRAP-PBNs display an energy- and endocytosis-independent internalization mechanism. In parallel, evaluation of the incubation conditions (LDH assay) revealed no effect on cell viability.

Graphs represent the mean ± SD of ≥ 2 independent experiments in triplicates (n≥6 individual values). Statistical evaluation using one-way ANOVA with Dunnett's post-test *versus* WRAP:siRNA-FLuc at 37°C revealed no significant (ns) differences between the other conditions using siRNA-FLuc. N.T. = not treated cells, siFLuc = siRNA for Firefly luciferase, siSCR = scrambled version.

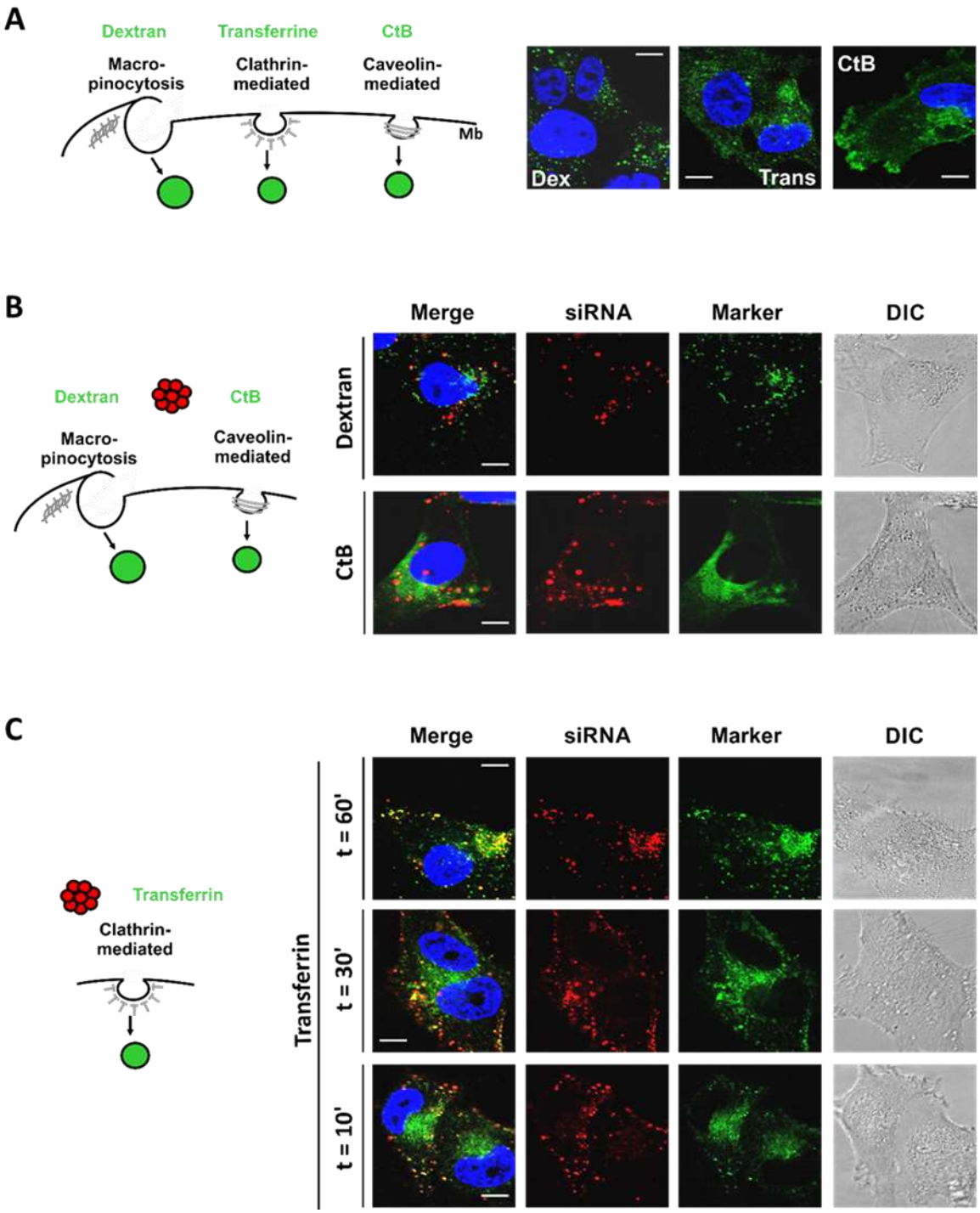

Figure 3: Evaluation of WRAP5:siRNA nanoparticle co-localization with markers of the endocytosis.
A. Schema of endocytosis markers and representative images of U87 cells as control experiment incubated with the three markers: Transferrin for clathrin-dependent endocytosis, cholera toxin subunit B (CtB) for caveolin-dependent endocytosis and dextran for macropinocytosis.
B. Representative images of U87 cells co-incubated with WRAP5:siRNA-Cy5 PBNs (with R=20 using 20 nM siRNA) and cholera toxin subunit B (CtB) or dextran, respectively, showing no co-localization of both compounds.
C. Representative images of U87 cells co-incubated with WRAP5:siRNA-Cy5 PBNs (with R=20 using 20 nM siRNA) and transferrin at different time points (10 min, 30 min and 60 min).
(A, B and **C)**. For each represented condition two independent experiments were performed and at least 10 arbitrary selected fields containing 3-5 cells were imaged. Bars represent 10 µm.

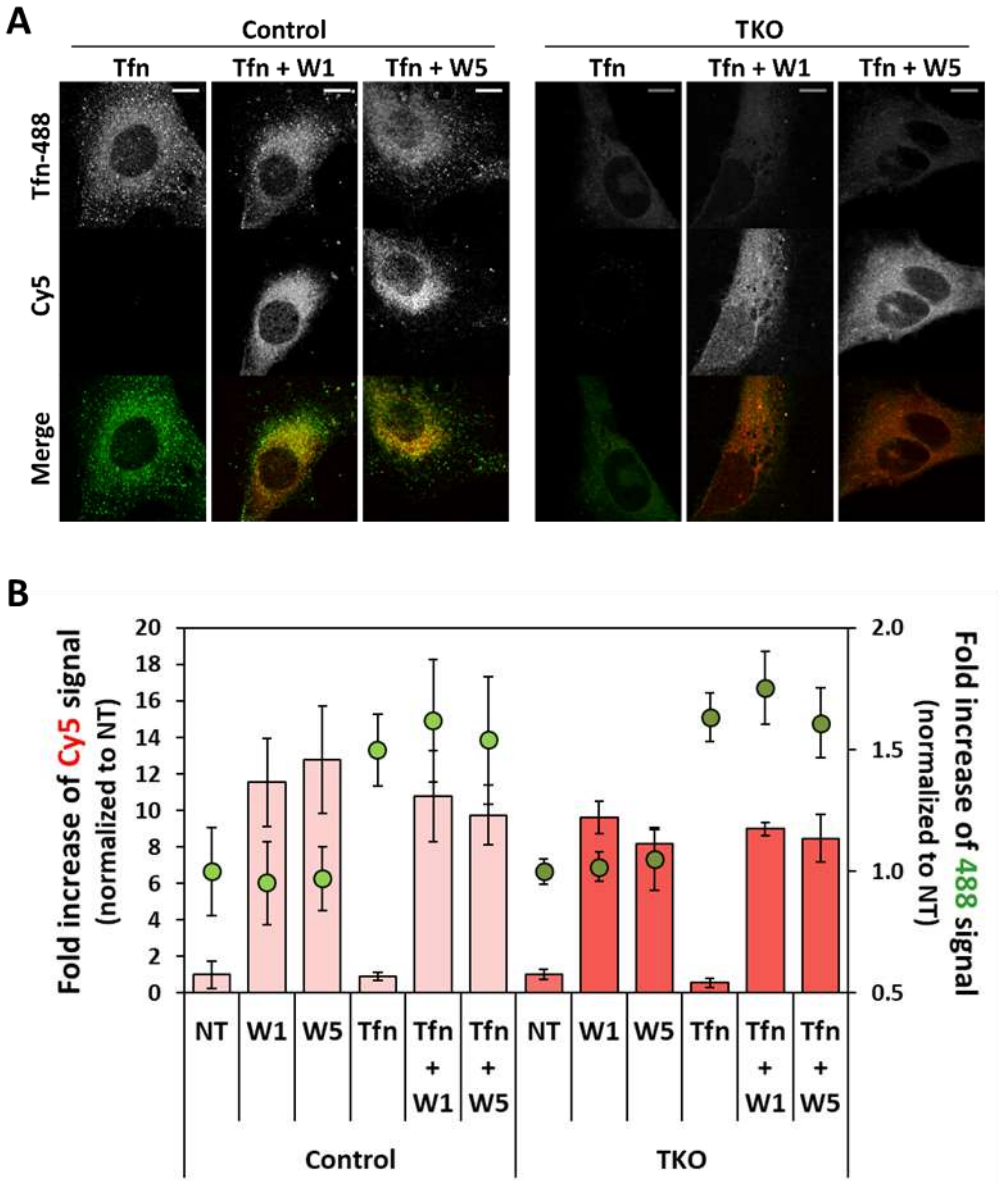

Figure 4. WRAP:siRNA nanoparticles internalized independently from dynamin-dependent pathways.

MEF cells were cultured under "normal" conditions (= Control) and under triple dynamin KO condition (= TKO) in parallel. Both cell types were pre-incubated with WRAP1:siRNA-Cy5 (W1) or WRAP5:siRNA (W5) with R = 20 using 40 nM siRNA followed by a transferrin-Alexa488 (Tfn) incubation.

A. After treatment, cells were fixed and fluorescence pictures were acquired by confocal spinning disc microscopy. Representative images showed an impaired internalization of fluorescent transferrin (slightly diffused versus strong punctuation) and a similar internalization pattern of the siRNA-Cy5 delivered in the cytosol independently of the condition. Bars represent 10 µm.

B. After incubation, cells were lysed and fluorescence values were recorded by fluorescence spectroscopy (siRNA-Cy5 and Tfn-488). Graph represents the mean ± SD of 3 independent experiments in duplicates (n≥6 individual values). NT = non-treated cells.

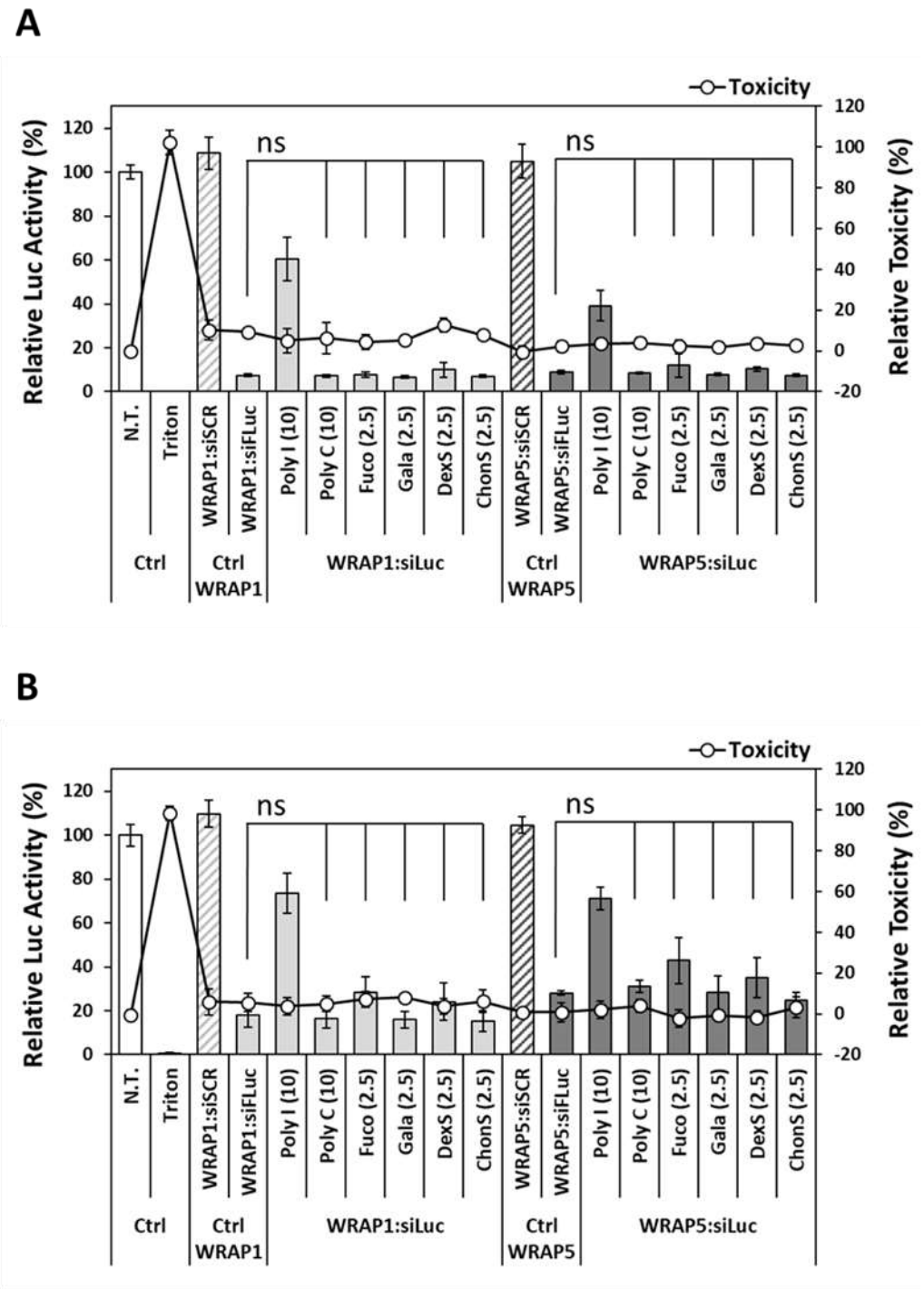

Figure 5: Effect of SR-A inhibitors on WRAP:siRNA nanoparticle activity.

Quantification of Luciferase silencing in U87 cells after incubation with the corresponding SR-A inhibitors and controls in the presence of WRAP:siRNA PBNs (with R=20 using 20 nM siRNA) in the absence of serum (**A**) or in the presence of serum (**B**). Graph represents the mean ± SD of 2 independent experiments in triplicates (n≥6 individual values). Concentration of the SR-A inhibitors and respective controls are given in brackets in µg/mL. Statistical evaluation using one-way ANOVA with Dunnett's post-test *versus* WRAP:siRNA-FLuc.

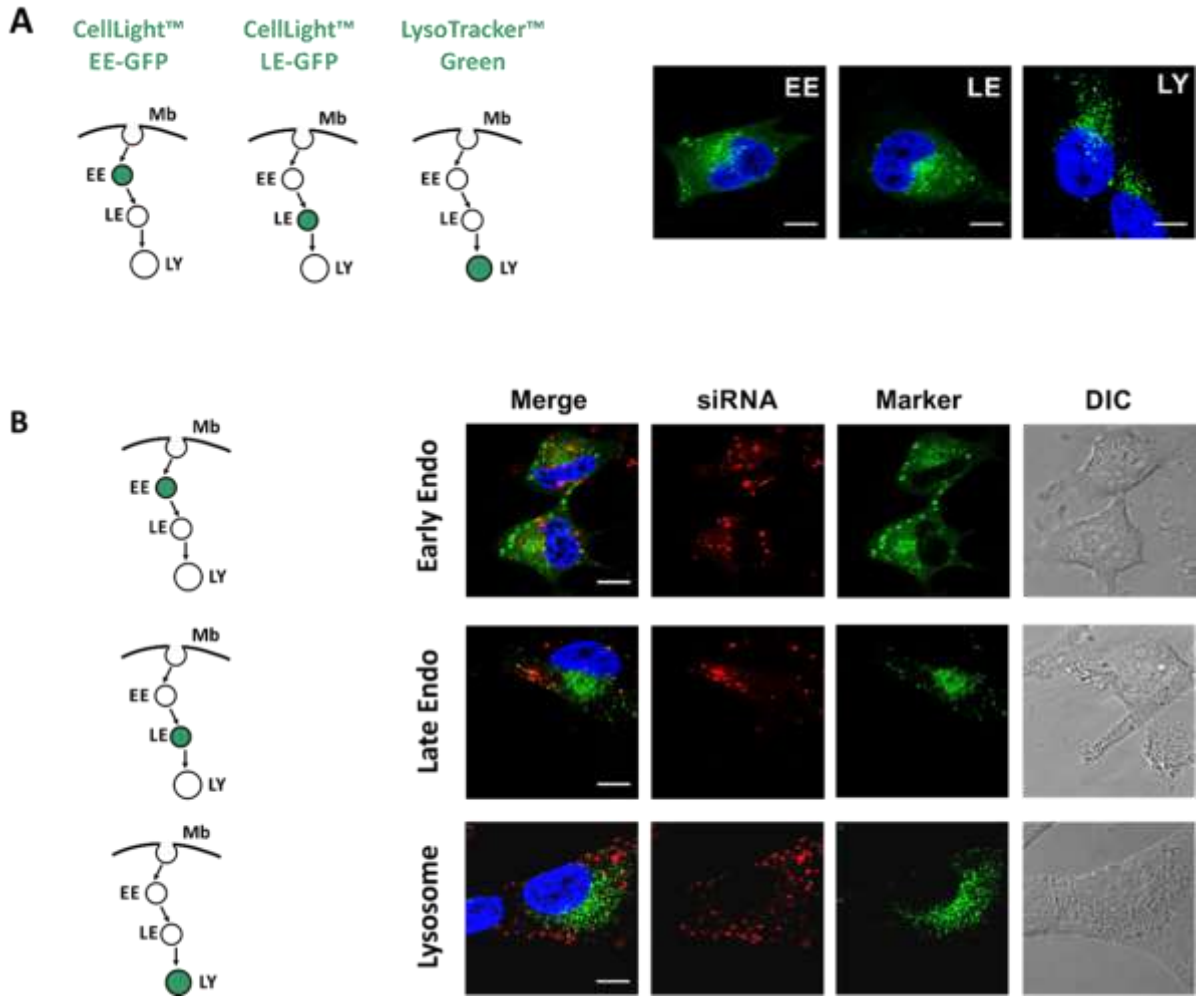

Figure 6: WRAP5:siRNA nanoparticles did not co-localize with endosomal and lysosomal markers after 1h incubation.

A. Schema and representative live cell images of U87 cells incubated with markers for early and late endosomes as well as for lysosomes.

B. Schema and representative live cell images of U87 cells incubated with WRAP5:siRNA-Cy5 PBNs (with R=20 using 20 nM siRNA) in the presence of early, late endosome and lysosome markers.

For each represented condition two independent experiments were performed and at least 10 arbitrary selected fields containing 3-5 cells were imaged. Bars represent 10 µm.

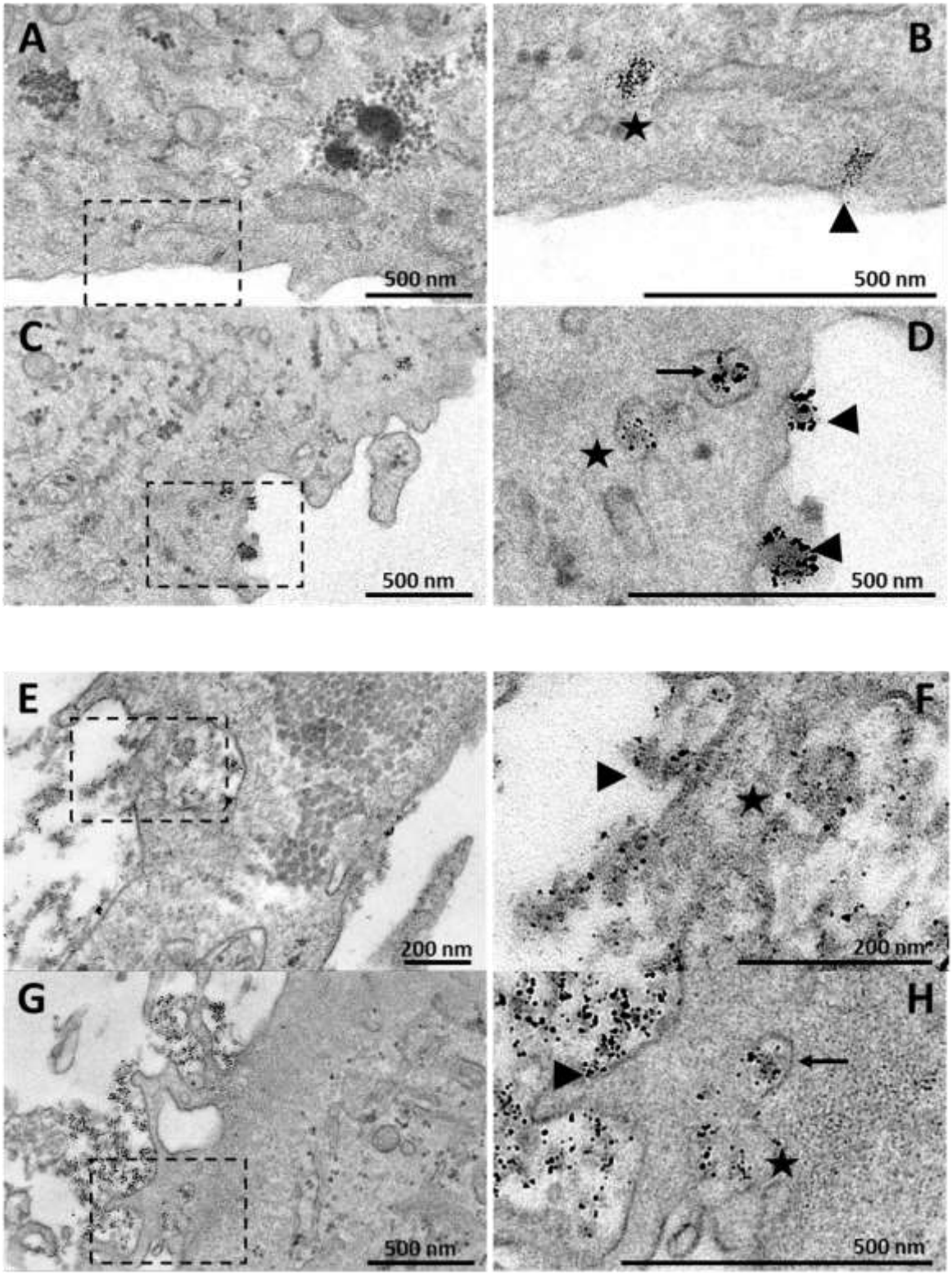

Figure 7: Evaluation of the internalization and cellular localization of the WRAP:siRNA nanoparticles by electron microscopy.

U87 cells were incubated with complexes of Nanogold™-labeled siRNA (siRNA-NG, 40 nM) complexed to WRAP5 (**A**, **B**, **C** and **D**) or to WRAP1 (**E**, **F**, **G** and **H**) at R=20 for 10-15 min (**A**, **B**, **E** and **F**) or 1-2h (**C**, **D**, **G** and **H**). WRAP:siRNA-NG complexes were visualized as dense particles at the plasma membrane (triangles), in endosomal vesicle (arrows) or free in cytosol (star).

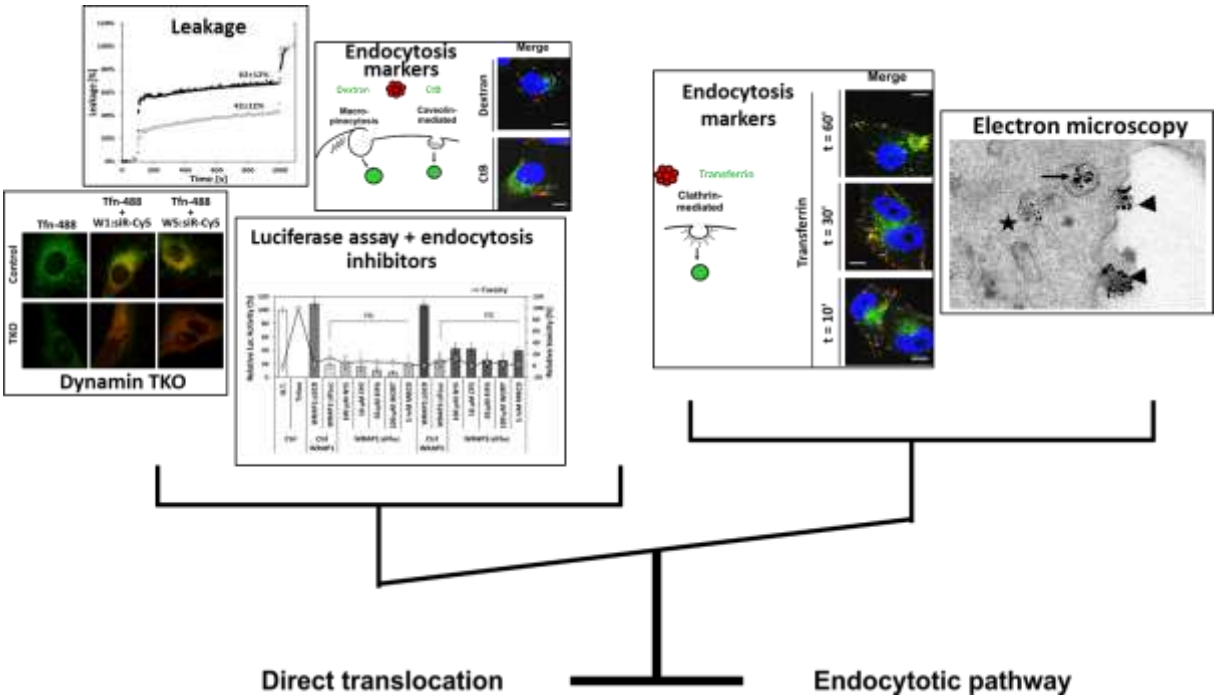

Figure 8: Concluding schema highlighting WRAP:siRNA nanoparticle cellular internalization.
The presented results obtained in this study showed a combined internalization of the WRAP:siRNA nanoparticles based on direct translocation and endocytosis-dependent mechanisms.

References

[1] J. Yang, Patisiran for the treatment of hereditary transthyretin-mediated amyloidosis, Expert Rev. Clin. Pharmacol. 12 (2019) 95–99. https://doi.org/10.1080/17512433.2019.1567326.

[2] A. Fire, S. Xu, M.K. Montgomery, S.A. Kostas, S.E. Driver, C.C. Mello, Potent and specific genetic interference by double-stranded RNA in Caenorhabditis elegans, Nature. 391 (1998) 806–811. https://doi.org/10.1038/35888.

[3] J.P. Dassie, X.-Y. Liu, G.S. Thomas, R.M. Whitaker, K.W. Thiel, K.R. Stockdale, D.K. Meyerholz, A.P. McCaffrey, J.O. McNamara, P.H. Giangrande, Systemic administration of optimized aptamer-siRNA chimeras promotes regression of PSMA-expressing tumors, Nat. Biotechnol. 27 (2009) 839–849. https://doi.org/10.1038/nbt.1560.

[4] Y. Dong, D.J. Siegwart, D.G. Anderson, Strategies, design, and chemistry in siRNA delivery systems, Adv. Drug Deliv. Rev. (2019). https://doi.org/10.1016/j.addr.2019.05.004.

[5] C. Puisney, A. Baeza-Squiban, S. Boland, Mechanisms of Uptake and Translocation of Nanomaterials in the Lung, Adv. Exp. Med. Biol. 1048 (2018) 21–36. https://doi.org/10.1007/978-3-319-72041-8_2.

[6] A. Ahmad, J.M. Khan, S. Haque, Strategies in the design of endosomolytic agents for facilitating endosomal escape in nanoparticles, Biochimie. 160 (2019) 61–75. https://doi.org/10.1016/j.biochi.2019.02.012.

[7] L.I. Selby, C.M. Cortez-Jugo, G.K. Such, A.P.R. Johnston, Nanoescapology: progress toward understanding the endosomal escape of polymeric nanoparticles, Wiley Interdiscip. Rev. Nanomed. Nanobiotechnol. 9 (2017). https://doi.org/10.1002/wnan.1452.

[8] J. Hoyer, I. Neundorf, Peptide vectors for the nonviral delivery of nucleic acids, Acc. Chem. Res. 45 (2012) 1048–1056. https://doi.org/10.1021/ar2002304.

[9] U. Langel, ed., Cell-Penetrating Peptides, CRC Press, Boca Raton, 2007.

[10] J. Mueller, I. Kretzschmar, R. Volkmer, P. Boisguerin, Comparison of cellular uptake using 22 CPPs in 4 different cell lines, Bioconjug. Chem. 19 (2008) 2363–2374. https://doi.org/10.1021/bc800194e.

[11] K. Ramaker, M. Henkel, T. Krause, N. Röckendorf, A. Frey, Cell penetrating peptides: a comparative transport analysis for 474 sequence motifs, Drug Deliv. 25 (2018) 928–937. https://doi.org/10.1080/10717544.2018.1458921.

[12] R. Brock, The uptake of arginine-rich cell-penetrating peptides: putting the puzzle together, Bioconjug. Chem. 25 (2014) 863–868. https://doi.org/10.1021/bc500017t.

[13] A.T. Jones, E.J. Sayers, Cell entry of cell penetrating peptides: tales of tails wagging dogs, J. Controlled Release. 161 (2012) 582–591. https://doi.org/10.1016/j.jconrel.2012.04.003.

[14] D. Vercauteren, J. Rejman, T.F. Martens, J. Demeester, S.C. De Smedt, K. Braeckmans, On the cellular processing of non-viral nanomedicines for nucleic acid delivery: mechanisms and methods, J. Controlled Release. 161 (2012) 566–581. https://doi.org/10.1016/j.jconrel.2012.05.020.

[15] G. Tünnemann, R.M. Martin, S. Haupt, C. Patsch, F. Edenhofer, M.C. Cardoso, Cargo-dependent mode of uptake and bioavailability of TAT-containing proteins and peptides in living cells, FASEB J. 20 (2006) 1775–1784. https://doi.org/10.1096/fj.05-5523com.

[16] G. Aldrian, A. Vaissière, K. Konate, Q. Seisel, E. Vivès, F. Fernandez, V. Viguier, C. Genevois, F. Couillaud, H. Démèné, D. Aggad, A. Covinhes, S. Barrère-Lemaire, S. Deshayes, P. Boisguerin, PEGylation rate influences peptide-based nanoparticles mediated siRNA delivery in vitro and in vivo, J. Controlled Release. 256 (2017) 79–91. https://doi.org/10.1016/j.jconrel.2017.04.012.

[17] P. Boisguérin, S. Deshayes, M.J. Gait, L. O'Donovan, C. Godfrey, C.A. Betts, M.J.A. Wood, B. Lebleu, Delivery of therapeutic oligonucleotides with cell penetrating peptides, Adv. Drug Deliv. Rev. 87 (2015) 52–67. https://doi.org/10.1016/j.addr.2015.02.008.

[18] K. Konate, M.F. Lindberg, A. Vaissiere, C. Jourdan, G. Aldrian, E. Margeat, S. Deshayes, P. Boisguerin, Optimisation of vectorisation property: A comparative study for a secondary

amphipathic peptide, Int. J. Pharm. 509 (2016) 71–84. https://doi.org/10.1016/j.ijpharm.2016.05.030.
[19] A. Vaissière, G. Aldrian, K. Konate, M.F. Lindberg, C. Jourdan, A. Telmar, Q. Seisel, F. Fernandez, V. Viguier, C. Genevois, F. Couillaud, P. Boisguerin, S. Deshayes, A retro-inverso cell-penetrating peptide for siRNA delivery, J. Nanobiotechnology. 15 (2017) 34. https://doi.org/10.1186/s12951-017-0269-2.
[20] K. Konate, M. Dussot, G. Aldrian, A. Vaissière, V. Viguier, I.F. Neira, F. Couillaud, E. Vivès, P. Boisguerin, S. Deshayes, Peptide-Based Nanoparticles to Rapidly and Efficiently "Wrap “n Roll" siRNA into Cells,” Bioconjug. Chem. 30 (2019) 592–603. https://doi.org/10.1021/acs.bioconjchem.8b00776.
[21] M.-L. Jobin, M. Blanchet, S. Henry, S. Chaignepain, C. Manigand, S. Castano, S. Lecomte, F. Burlina, S. Sagan, I.D. Alves, The role of tryptophans on the cellular uptake and membrane interaction of arginine-rich cell penetrating peptides, Biochim. Biophys. Acta. 1848 (2015) 593–602. https://doi.org/10.1016/j.bbamem.2014.11.013.
[22] R.J. Park, H. Shen, L. Liu, X. Liu, S.M. Ferguson, P. De Camilli, Dynamin triple knockout cells reveal off target effects of commonly used dynamin inhibitors, J. Cell Sci. 126 (2013) 5305–5312. https://doi.org/10.1242/jcs.138578.
[23] R. Maget-Dana, The monolayer technique: a potent tool for studying the interfacial properties of antimicrobial and membrane-lytic peptides and their interactions with lipid membranes, Biochim. Biophys. Acta. 1462 (1999) 109–140.
[24] P. Arukuusk, L. Pärnaste, N. Oskolkov, D.-M. Copolovici, H. Margus, K. Padari, K. Möll, J. Maslovskaja, R. Tegova, G. Kivi, A. Tover, M. Pooga, M. Ustav, U. Langel, New generation of efficient peptide-based vectors, NickFects, for the delivery of nucleic acids, Biochim. Biophys. Acta. 1828 (2013) 1365–1373. https://doi.org/10.1016/j.bbamem.2013.01.011.
[25] P. Säälik, K. Padari, A. Niinep, A. Lorents, M. Hansen, E. Jokitalo, U. Langel, M. Pooga, Protein delivery with transportans is mediated by caveolae rather than flotillin-dependent pathways, Bioconjug. Chem. 20 (2009) 877–887. https://doi.org/10.1021/bc800416f.
[26] K. Konate, L. Crombez, S. Deshayes, M. Decaffmeyer, A. Thomas, R. Brasseur, G. Aldrian, F. Heitz, G. Divita, Insight into the cellular uptake mechanism of a secondary amphipathic cell-penetrating peptide for siRNA delivery, Biochemistry (Mosc.). 49 (2010) 3393–3402. https://doi.org/10.1021/bi901791x.
[27] K. Cleal, L. He, P.D. Watson, A.T. Jones, Endocytosis, intracellular traffic and fate of cell penetrating peptide based conjugates and nanoparticles, Curr. Pharm. Des. 19 (2013) 2878–2894. https://doi.org/10.2174/13816128113199990297.
[28] J.D. Ramsey, N.H. Flynn, Cell-penetrating peptides transport therapeutics into cells, Pharmacol. Ther. 154 (2015) 78–86. https://doi.org/10.1016/j.pharmthera.2015.07.003.
[29] A.I. Ivanov, Pharmacological inhibition of endocytic pathways: is it specific enough to be useful?, Methods Mol. Biol. Clifton NJ. 440 (2008) 15–33. https://doi.org/10.1007/978-1-59745-178-9_2.
[30] D. Vercauteren, R.E. Vandenbroucke, A.T. Jones, J. Rejman, J. Demeester, S.C. De Smedt, N.N. Sanders, K. Braeckmans, The Use of Inhibitors to Study Endocytic Pathways of Gene Carriers: Optimization and Pitfalls, Mol. Ther. 18 (2010) 561–569. https://doi.org/10.1038/mt.2009.281.
[31] C. Rosazza, H. Deschout, A. Buntz, K. Braeckmans, M.-P. Rols, A. Zumbusch, Endocytosis and Endosomal Trafficking of DNA After Gene Electrotransfer In Vitro, Mol. Ther. Nucleic Acids. 5 (2016) e286. https://doi.org/10.1038/mtna.2015.59.
[32] S. Dixit, T. Novak, K. Miller, Y. Zhu, M.E. Kenney, A.-M. Broome, Transferrin receptor-targeted theranostic gold nanoparticles for photosensitizer delivery in brain tumors, Nanoscale. 7 (2015) 1782–1790. https://doi.org/10.1039/c4nr04853a.
[33] V. Haucke, M.M. Kozlov, Membrane remodeling in clathrin-mediated endocytosis, J. Cell Sci. 131 (2018). https://doi.org/10.1242/jcs.216812.
[34] M. Kaksonen, A. Roux, Mechanisms of clathrin-mediated endocytosis, Nat. Rev. Mol. Cell Biol. 19 (2018) 313–326. https://doi.org/10.1038/nrm.2017.132.

[35] S.M. Ferguson, P. De Camilli, Dynamin, a membrane-remodelling GTPase, Nat. Rev. Mol. Cell Biol. 13 (2012) 75–88. https://doi.org/10.1038/nrm3266.
[36] S.M. Ferguson, S. Ferguson, A. Raimondi, S. Paradise, H. Shen, K. Mesaki, A. Ferguson, O. Destaing, G. Ko, J. Takasaki, O. Cremona, E. O' Toole, P. De Camilli, Coordinated actions of actin and BAR proteins upstream of dynamin at endocytic clathrin-coated pits, Dev. Cell. 17 (2009) 811–822. https://doi.org/10.1016/j.devcel.2009.11.005.
[37] M. Rosendale, T.N.N. Van, D. Grillo-Bosch, S. Sposini, L. Claverie, I. Gauthereau, S. Claverol, D. Choquet, M. Sainlos, D. Perrais, Functional recruitment of dynamin requires multimeric interactions for efficient endocytosis, Nat. Commun. 10 (2019) 4462. https://doi.org/10.1038/s41467-019-12434-9.
[38] K. Ezzat, H. Helmfors, O. Tudoran, C. Juks, S. Lindberg, K. Padari, S. El-Andaloussi, M. Pooga, U. Langel, Scavenger receptor-mediated uptake of cell-penetrating peptide nanocomplexes with oligonucleotides, FASEB J. Off. Publ. Fed. Am. Soc. Exp. Biol. 26 (2012) 1172–1180. https://doi.org/10.1096/fj.11-191536.
[39] K.-L. Veiman, I. Mäger, K. Ezzat, H. Margus, T. Lehto, K. Langel, K. Kurrikoff, P. Arukuusk, J. Suhorutšenko, K. Padari, M. Pooga, T. Lehto, Ü. Langel, PepFect14 peptide vector for efficient gene delivery in cell cultures, Mol. Pharm. 10 (2013) 199–210. https://doi.org/10.1021/mp3003557.
[40] H. Helmfors, S. Lindberg, Ü. Langel, SCARA Involvement in the Uptake of Nanoparticles Formed by Cell-Penetrating Peptides, Methods Mol. Biol. Clifton NJ. 1324 (2015) 163–174. https://doi.org/10.1007/978-1-4939-2806-4_11.
[41] K. Ezzat, Y. Aoki, T. Koo, G. McClorey, L. Benner, A. Coenen-Stass, L. O'Donovan, T. Lehto, A. Garcia-Guerra, J. Nordin, A.F. Saleh, M. Behlke, J. Morris, A. Goyenvalle, B. Dugovic, C. Leumann, S. Gordon, M.J. Gait, S. El-Andaloussi, M.J.A. Wood, Self-Assembly into Nanoparticles Is Essential for Receptor Mediated Uptake of Therapeutic Antisense Oligonucleotides, Nano Lett. 15 (2015) 4364–4373. https://doi.org/10.1021/acs.nanolett.5b00490.
[42] C.C. Scott, F. Vacca, J. Gruenberg, Endosome maturation, transport and functions, Semin. Cell Dev. Biol. 31 (2014) 2–10. https://doi.org/10.1016/j.semcdb.2014.03.034.
[43] N. Naslavsky, S. Caplan, The enigmatic endosome - sorting the ins and outs of endocytic trafficking, J. Cell Sci. 131 (2018). https://doi.org/10.1242/jcs.216499.
[44] M. Anko, J. Majhenc, K. Kogej, R. Sillard, Ü. Langel, G. Anderluh, M. Zorko, Influence of stearyl and trifluoromethylquinoline modifications of the cell penetrating peptide TP10 on its interaction with a lipid membrane, Biochim. Biophys. Acta - Biomembr. 1818 (2012) 915–924. https://doi.org/10.1016/j.bbamem.2011.12.028.
[45] M. Jafari, D.N. Karunaratne, C.M. Sweeting, P. Chen, Modification of a designed amphipathic cell-penetrating peptide and its effect on solubility, secondary structure, and uptake efficiency, Biochemistry (Mosc.). 52 (2013) 3428–3435. https://doi.org/10.1021/bi4001326.
[46] F.S. Hassane, R. Abes, S. El Andaloussi, T. Lehto, R. Sillard, U. Langel, B. Lebleu, Insights into the cellular trafficking of splice redirecting oligonucleotides complexed with chemically modified cell-penetrating peptides, J. Controlled Release. 153 (2011) 163–172. https://doi.org/10.1016/j.jconrel.2011.04.013.
[47] S. Pujals, J. Fernández-Carneado, C. López-Iglesias, M.J. Kogan, E. Giralt, Mechanistic aspects of CPP-mediated intracellular drug delivery: relevance of CPP self-assembly, Biochim. Biophys. Acta. 1758 (2006) 264–279. https://doi.org/10.1016/j.bbamem.2006.01.006.
[48] R. Wattiaux, N. Laurent, S. Wattiaux-De Coninck, M. Jadot, Endosomes, lysosomes: their implication in gene transfer, Adv. Drug Deliv. Rev. 41 (2000) 201–208.
[49] S. Lindberg, J. Regberg, J. Eriksson, H. Helmfors, A. Muñoz-Alarcón, A. Srimanee, R.A. Figueroa, E. Hallberg, K. Ezzat, Ü. Langel, A convergent uptake route for peptide- and polymer-based nucleotide delivery systems, J. Controlled Release. 206 (2015) 58–66. https://doi.org/10.1016/j.jconrel.2015.03.009.

[50] C. Juks, A. Lorents, P. Arukuusk, Ü. Langel, M. Pooga, Cell-penetrating peptides recruit type A scavenger receptors to the plasma membrane for cellular delivery of nucleic acids, FASEB J. Off. Publ. Fed. Am. Soc. Exp. Biol. 31 (2017) 975–988. https://doi.org/10.1096/fj.201600811R.
[51] A. Walrant, A. Bauza, C. Girardet, I.D. Alves, S. Lecomte, F. Illien, S. Cardon, N. Chaianantakul, M. Pallerla, F. Burlina, A. Frontera, S. Sagan, Ionpair-π interactions favor cell penetration of arginine/tryptophan-rich cell-penetrating peptides, (2019). https://doi.org/10.1101/717207.
[52] F. Duchardt, M. Fotin-Mleczek, H. Schwarz, R. Fischer, R. Brock, A Comprehensive Model for the Cellular Uptake of Cationic Cell-penetrating Peptides, Traffic. 8 (2007) 848–866. https://doi.org/10.1111/j.1600-0854.2007.00572.x.
[53] S. Watanabe, E. Boucrot, Fast and ultrafast endocytosis, Curr. Opin. Cell Biol. 47 (2017) 64–71. https://doi.org/10.1016/j.ceb.2017.02.013.
[54] E. Vives, Cellular uptake [correction of utake] of the Tat peptide: an endocytosis mechanism following ionic interactions, J. Mol. Recognit. JMR. 16 (2003) 265–271. https://doi.org/10.1002/jmr.636.

SUPPLEMENT MATERIAL

MATERIALS AND METHODS

Materials: Dioleylphosphatidylglycerol (DOPG) and dioleylphosphatidylcholine (DOPC) phospholipids, cholesterol (Chol), sphingomyelin (SM), dioleoyl-phosphatidylethanolamine (DOPE), phosphatedylinositol from soybean (PI) and bis(monooleoylglycero) phosphate (LBPA) were purchased from Avanti Polar Lipids. WRAP1 (NH_2-LLWRLWRLLWRLWRLL-$CONH_2$) and WRAP5 (NH_2-LLRLLRWWWRLLRLL-$CONH_2$) peptides were synthesized on the SynBio3 platform and crude products were purified in house following a qualitative analysis by HPLC/MS. Unlabeled and Cy5-labeled siRNA (siFLuc: 5'-CUU-ACG-CUG-AGU-ACU-UCG-AdTdT-'3 as sense strand) were purchased from Eurogentec. The following cell lines were used: Human glioblastoma cell line (U87, $Fluc^+$) (Aldrian et al., 2017) and dynamin-triple KO murine endothelium fibroblast (TKO-MEF) (Park et al., 2013). The following products were purchased from Sigma-Aldrich: glucose, sodium azide (NaN_3), 2-deoxy-glucose (DG), polyinosinic acid (Poly I), polycytidylic acid (Poly C), Dextran sulfate, Chondroitin sulfate, Fucoidan and Galactose. The following endocytosis inhibitors were used: nystatin (NYS), chlorpromazine (CPZ), 5-(N-ethyl-N-isopropyl)-amiloride (EIPA), wortmanin (WORT), methyl-β-cyclodextrin (MBCD) and NaN_3/2-Desoxy-Glucose (for ATP depletion) (all from Sigma-Aldrich). Transferrin-Alexa488 (clathrin-dependent endocytosis), Cholera Toxin Subunit B-Alexa488 (CtB, caveolin-dependent endocytosis) and pHrodo™ Green Dextran 10.000 MW-green (micropinocytosis) were used as endocytosis markers (all from ThermoFisher Scientific). The following vesicle markers were used: CellLight™ Early Endosomes-GFP, BacMam 2.0, CellLight™ Late Endosomes-GFP, BacMam 2.0, LysoTracker™ Green DND-26 (all from ThermoFisher Scientific).

Leakage assay on LUV reflecting the plasma membrane: Large unilamellar vesicles (LUV) composed of DOPC/SM/Chol (4/4/2; mol/mol/mol) were prepared by removing organic solvent (evaporation for 45-60 min at 60°C). Thereafter, the lipids were hydrated in a buffer (20 mM HEPES, 75 mM NaCl, pH 7.4) containing 12.5 mM ANTS fluorescent dye (8-aminonaphthalene-1,3,6-trisulfonic acid, disodium salt; Invitrogen) together with 45 mM DPX quencher (p-xylene-bispyridinium bromide; Invitrogen). The suspension was vigorously agitated with a Vortex (30 s), freeze-thawed 5 times and then extruded 21 times through two stacked 100 nm polycarbonate filters (Nucleopore, Whatman). Free dye and quencher were removed by gel filtration (G50-sepharose, Amersham Biosciences). LUV concentration was assessed using the LabAssay Phospholipid kit (Wako) as described by the manufacturer and LUV mean size was determined by Dynamic Light Scattering (DLS, NanoZS, Malvern).

Fluorescence leakage assay was measured on a PTI spectrofluorometer at room temperature (Ex = 360 nm $\pm$ 3 nm; Em 530 nm $\pm$ 5 nm). In details, LUVs were diluted in 1 mL buffer (20 mM HEPES, 145 mM

NaCl, pH 7.4) to a final concentration of 100 µM. To access the background fluorescence, the LUVs alone were measured during 100 seconds. Thereafter, leakage was measured as an increase in fluorescence intensity upon addition of WRAP1/WRAP5 (2.5 µM) or WRAP1/WRAP5-based nanoparticle (R = 20 using 2.5 µM WRAP) during the next following 900 seconds (15 min). Finally, 100% fluorescence was achieved by solubilizing the membranes with 0.1% (v/v) Triton X-100 resulting in a completely unquenched probe (at 1,000 seconds). Relative percentage of leakage was calculated using the following equation: [(exp. value – minimal value) / (maximal triton value – minimal value)] x 100.

Leakage assay on LUV reflecting the endosomes: Large unilamellar vesicles (LUV) composed of DOPC/DOPE/PI/LBPA (5/2/1/2; mol/mol/mol/mol) were prepared by removing organic solvent (evaporation for 45-60 min at 60°C). Thereafter, the lipids were hydrated in a buffer (20 mM 2-(N-morpholino)ethanesulfonic acid (MES), 145 mM NaCl, pH 5.5) containing 12.5 mM ANTS fluorescent dye (8-aminonaphthalene-1,3,6-trisulfonic acid, disodium salt; Invitrogen) together with 45 mM DPX quencher (p-xylene-bispyridinium bromide; Invitrogen). The suspension was vigorously agitated with a Vortex (30 s), freeze-thawed 5 times and then extruded 21 times through two stacked 100 nm polycarbonate filters (Nucleopore, Whatman). Free dye and quencher were removed by gel filtration (G50-sepharose, Amersham Biosciences). LUV concentration was assessed using the LabAssay Phospholipid kit (Wako) as described by the manufacturer and LUV mean size was determined by Dynamic Light Scattering (DLS, NanoZS, Malvern).

Fluorescence leakage assay was measured on a PTI spectrofluorometer at room temperature (Ex = 360 nm $\pm$ 3 nm; Em 530 nm $\pm$ 5 nm) as described below.

Luciferase assay. U87 cells (5,000 cells per well) were seeded 24 h before experiment into 96-well plates using the corresponding medium as described above. Nanoparticles were formed by mixing siRNA and CPPs in 5% glucose water as previously described (Konate et al., 2019) followed by an incubation of a 5-10 min warming step at 37°C prior incubation with the cells. Before the nanoparticle incubation, the cell growth medium was replaced by 70 µL of fresh pre-warmed serum-free DMEM. Afterwards, 30 µL of the nanoparticle solutions were added directly to the medium recovering the cells and incubated 1.5 h at 37°C. Finally, the whole medium solution was replaced by 200 µL of fresh DMEM supplemented with 10 % FBS and the cells were incubated for further 36 h. The medium covering the cells was then carefully removed and 50 µL of 0.5 X Passive Lysis Buffer (PLB; Promega) were added and the plates were shaken for 30 min at 4°C. After a centrifugation step (10 min, 1,800 rpm, 4°C), 5 µL of each cell lysate supernatant were transferred into a white 96-well plate (Greiner Lumitrac^{TM} 200). Luciferase activity was quantified using a plate-reading luminometer (POLARstar Omega, BMG Labtech) using half-diluted Dual Luciferase Assay Reagents as described by the manufacturer (Promega). The results were expressed as percentage of relative light units (RLU) for each luciferase,

normalized first to non-treated cells (%FLuc and %NLuc) and then normalized to the value of %NLuc to obtain the Relative Luc Activity (%FLuc/%NLuc).

Cytotoxicity assay (LDH). The Cytotoxicity Detection Kit^{Plus} (LDH, Roche Diagnostics) was used to evaluate the cytotoxicity induced by the nanoparticles. After the nanoparticle incubation (36 h), at least one well was used as a LDH positive control (100% toxicity) by adding Triton X-100 (Sigma-Aldrich) to a final concentration of 0.1% (~15 min incubation at 37°C). Afterwards, 50 µL supernatant of each well were transferred in a new clear 96-well plate (Greiner) and completed with 50 µL of the "dye solution/catalyst" mixture. The plate was then incubated in the darkness for 30 min at room temperature. Reaction was stopped by adding 25 µL of HCl (1 N) to each well before measuring the absorption at 490 nm using the POLARstar Omega plate reader (BMG Labtech). Relative toxicity (%) was calculated with the following formula: [(exp. value – value non-treated cells) / (value triton – value non-treated cells)] x 100.

Confocal microscopy. 300,000 U87 cells were seeded 24 h before imaging into 35 mm glass bottom dishes (FluoroDish, World Precision Instruments). Before experiments, cells were washed twice with D-PBS and covered with 1,600 µL of FluoroBrite DMEM medium (Life Technologies). Afterwards, 400 µL of nanoparticles (peptide:Cy5-siRNA; R = 20, Cy5-siRNA = 20 nM), formulated in an aqueous solution of 5% glucose were directly added on the cells for the indicated time periods. 10 min before the end of the nanoparticle incubation, Hoechst 33342 dye (Sigma-Aldrich) was added to the cell for nucleus labeling. Afterwards, cells were washed twice with D-PBS and covered with FluoroBrite DMEM medium (Life Technologies). Live cell images were acquired on an inverted Leica SP5-SMD microscope using a lens 63x/1.4 NA oil. For all acquisition settings, the main excitation source for confocal mode was a 405 nm diode and a 633 nm helium/neon laser. The specific parameters for each fluorophore were: Hoechst dye, excitation at 405 nm, detection between 415 nm - 485 nm; Cy5 excitation at 633 nm and detection between 655 nm - 685 nm. Image acquisition was done sequentially to minimize crosstalk between the fluorophores. Each confocal image was merged and adjusted with the same brightness and contrast parameters using the ImageJ software.

Agarose gel shift assay. WRAP:siRNA complexes [siRNA = 10 µM in 20 µL of an aqueous solution containing 5% glucose] were formed at different ratios and pre-incubated for 30 min at room temperature. Then 3 µL of the SCARA inhibitors were added to the complex solution in order to obtain a final concentration of Poly I = 10 µg/mL, Fuco = 2.5 µg/mL and DexS = 2.5 µg/mL. After a second incubation time of 30 min at room temperature, 20 µL of each solution were loaded on an agarose gel (1 % w/v, Sigma-Aldrich) and electrophoresis was performed at 50 V for 25 min. To visualize the siRNA the agarose gel was stained with GelRed (Interchim) for UV detection.

ADDITIONAL FIGURES

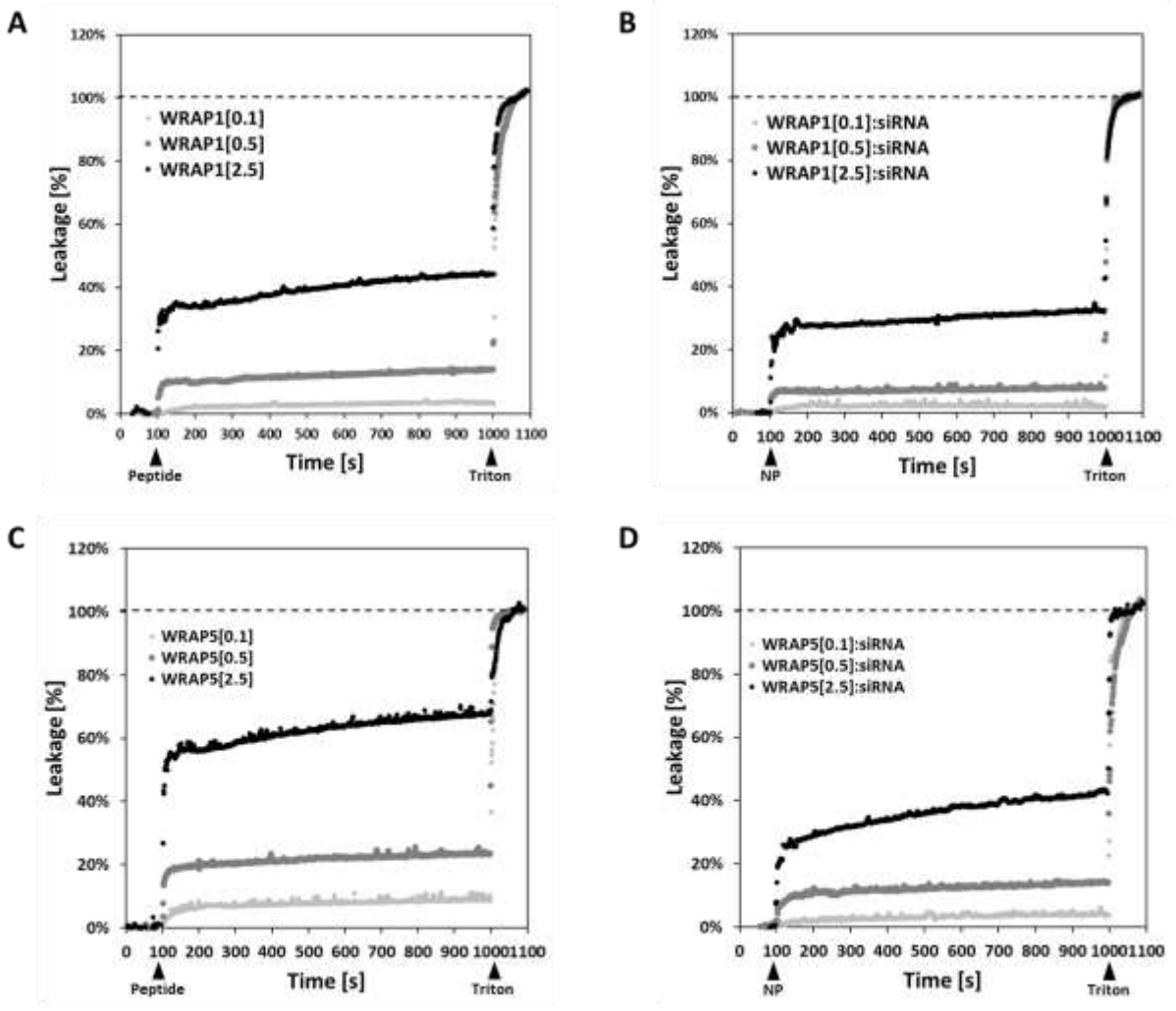

Figure S1: Evaluation of dose-dependent leakage properties of WRAP peptides and WRAP:siRNA nanoparticles.

Comparison of the leakage properties of WRAP alone (0.1, 0.5 or 2.5 µM) (**A and C**) and WRAP:siRNA PBNs (R=20, with a peptide concentration of 0.1, 0.5 or 2.5 µM) on LUVs [DOPC/SM/Chol (2:2:1)] (**B and D**). Peptides/nanoparticles were injected at 100 s and the Triton (positive control) at 1000 s (n ≥ 4).

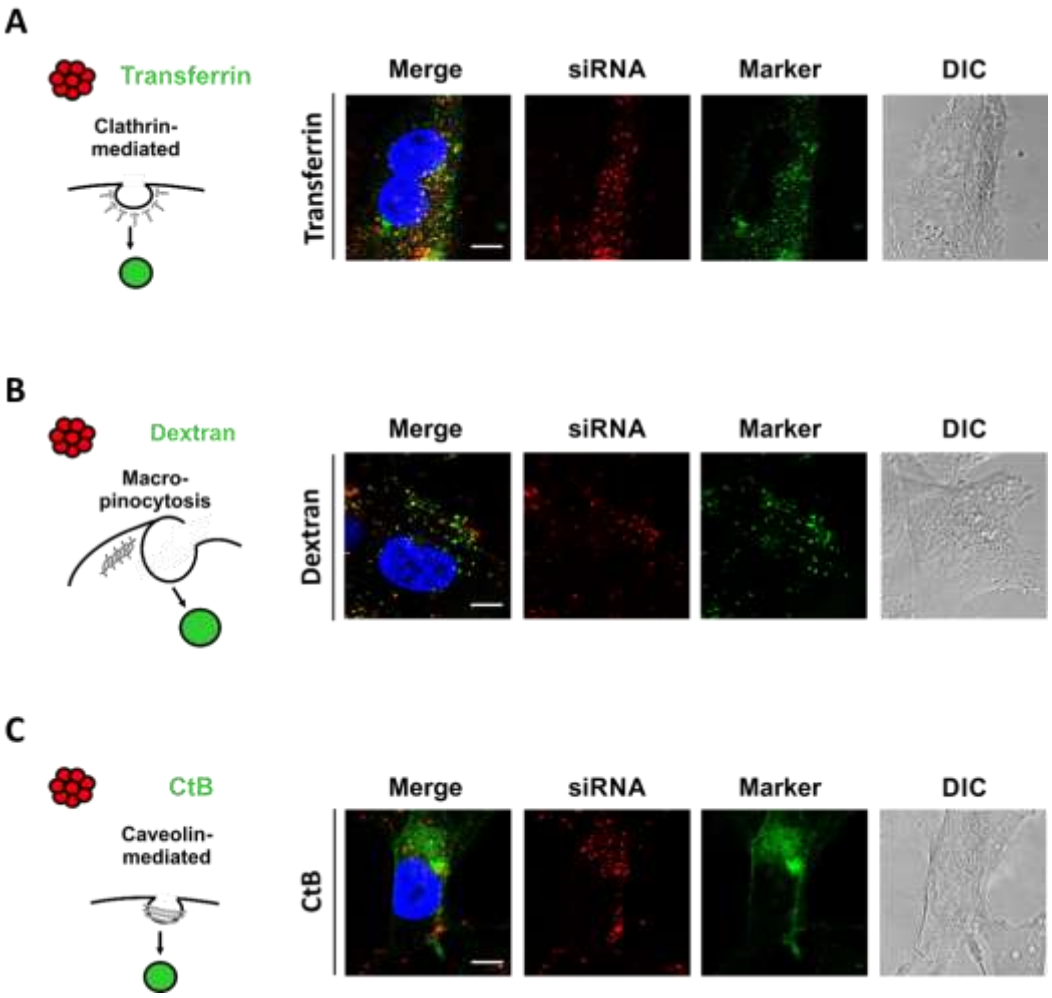

Figure S2: Evaluation of WRAP1:siRNA nanoparticle co-localization with markers of the endocytosis. Schema of endocytosis markers and representative images of U87 cells co-incubated with WRAP1:siRNA-Cy5 PBNs (with R=20 using 20 nM siRNA) and transferrin (**A**), dextran (**B**) or cholera toxin subunit B (CtB) (**C**).

Dextran and Ctb showed no co-localization whereas transferrin revealed the same amount of co-localization with siRNA-Cy5 as demonstrated for WRAP5:siRNA-Cy5 PBNs incubation (see **Figure 3C**). Bars represent 10 µm.

(A, B and **C)**. For each represented condition two independent experiments were performed and at least 10 arbitrary selected fields containing 3-5 cells were imaged. Bars represent 10 µm.

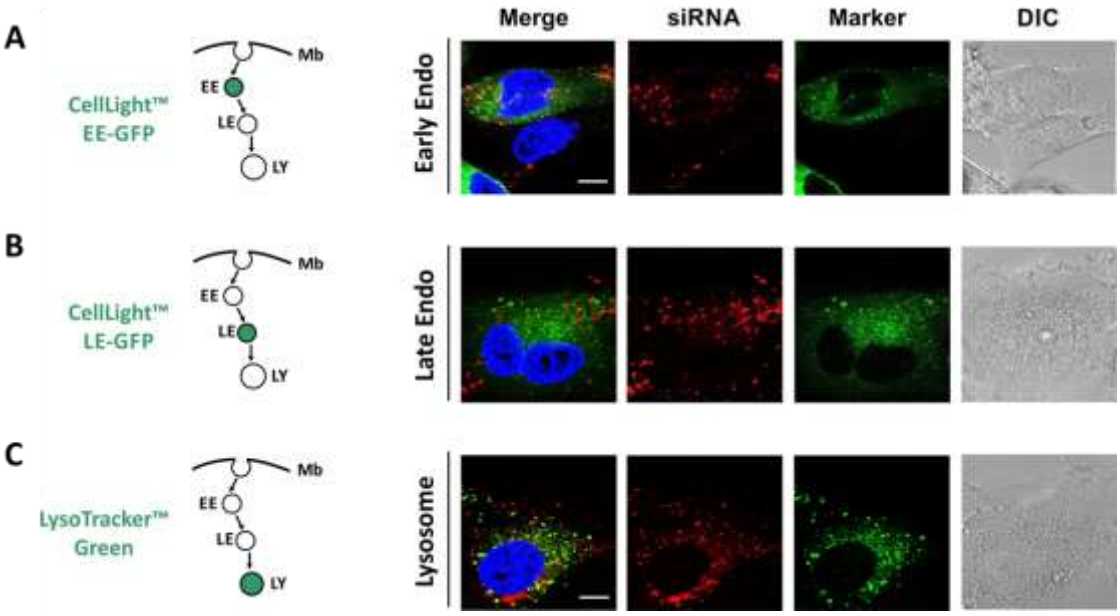

Figure S3: WRAP1:siRNA nanoparticles did not co-localize with endosomal and lysosomal markers after 1h incubation.

Schema and representative live cell images of U87 cells incubated with WRAP1:siRNA-Cy5 PBNs (with R=20 using 20 nM siRNA) in co-incubation with early (**A**), late endosomes (**B**) and lysosome (**C**) markers (60 min incubation).

EE and LE markers showed no co-localization whereas the lysosome marker revealed the same amount of co-localization with siRNA-Cy5 as demonstrated for WRAP1:siRNA-Cy5 PBNs incubation (see **Figure 6C**).

(A, B and **C)**. For each represented condition two independent experiments were performed and at least 10 arbitrary selected fields containing 3-5 cells were imaged. Bars represent 10 µm.

Bars represent 10 µm.

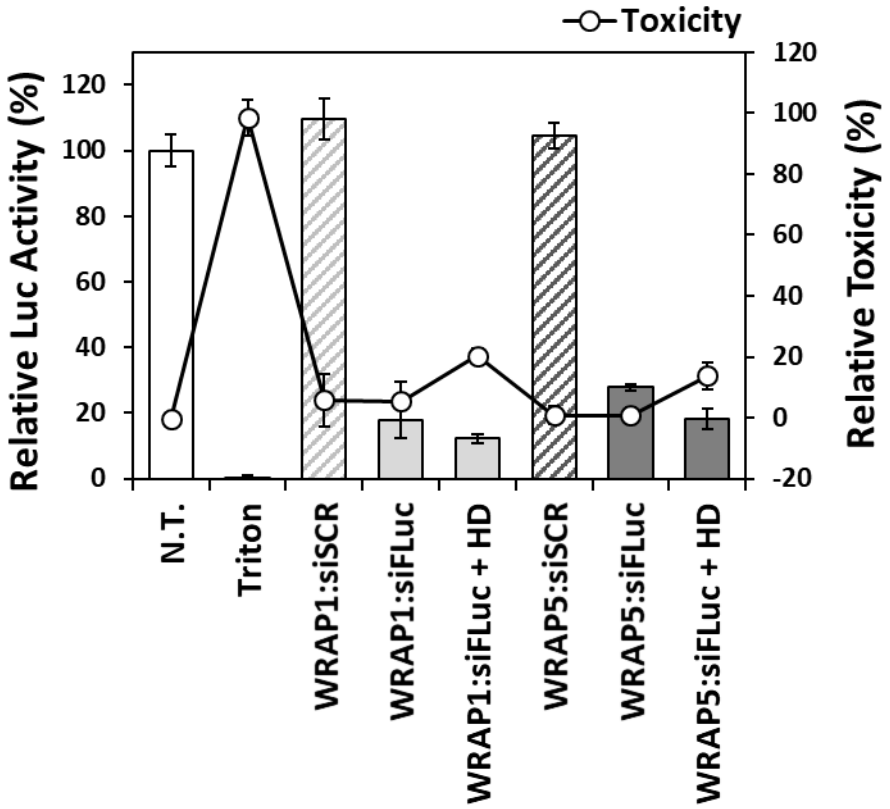

Figure S4: Hydroxy-dynasore did not reduce silencing properties of WRAP:siRNA nanoparticles.
Quantification of Luciferase silencing in U87 cells after incubation with hydroxyl dynasore and control conditions in the presence of WRAP:siRNA PBNs (with R=20 using 20 nM siRNA).
In the presence of hydroxyl-dynasore luciferase silencing property of siRNA-loaded WRAP-PBNs was identic as the control condition without the dynamin inhibitor. This knock-down efficiency was specific because nanoparticles formulated with a scrambled siRNA version revealed no luciferase silencing. In parallel evaluation of the incubation conditions (LDH assay) revealed only slight effect on cell viability (>20%). Graph represents the mean ± SD of 2 independent experiments in triplicates (n≥6 individual values).

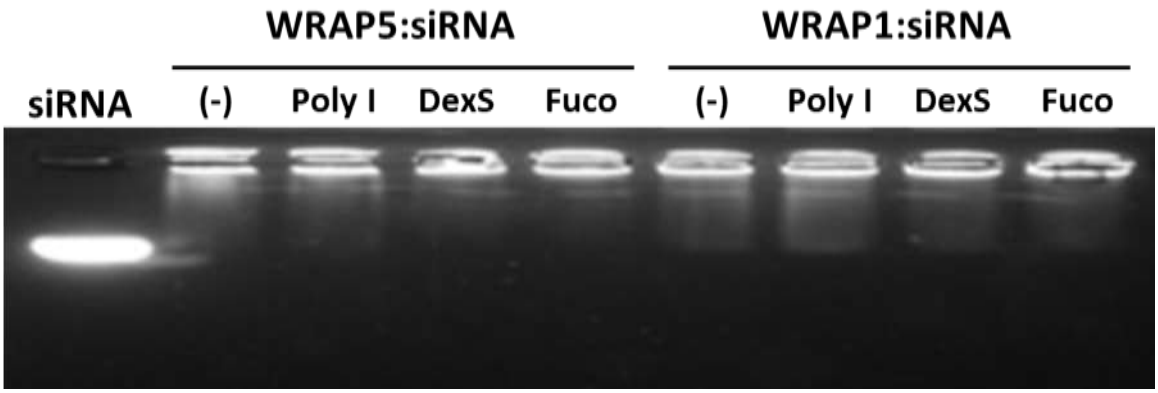

Figure S5: Effect of SCARA inhibitors on WRAP:siRNA nanoparticle stability.
B. Gel shift assay with Poly I = polyinosinic acid (10 µg/mL), Fuco = fucoidan (2.5 µg/mL) and DexS = dextran sulfate (2.5 µg/mL) to demonstrate that the poly-anions did not destabilize WRAP:siRNA nanoparticles.

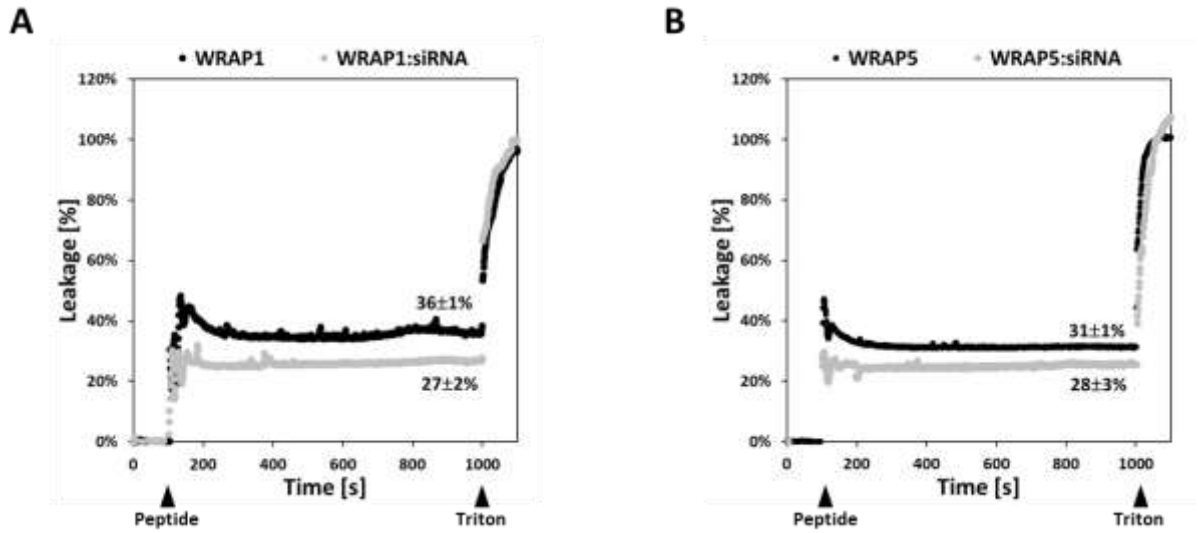

Figure S6: WRAP peptides and WRAP nanoparticles interact with LUVs reflecting the endosomal membrane composition.

A. Comparison of the leakage properties of WRAP1 alone (2.5 µM) and WRAP1:siRNA (2.5 µM:125 nM) PBNs on LUVs [DOPC/DOPE/PI/LBPA (5:2:1:2)].

B. Comparison of the leakage properties of WRAP5 alone (2.5 µM) and WRAP5:siRNA (2.5 µM:125 nM) PBNs on LUVs [DOPC/DOPE/PI/LBPA (5:2:1:2)].

Peptides/nanoparticles were injected at 100 s and the Triton (positive control) at 1000 s (n = 2).